Master's thesis
Solid Earth Geophysics

Enhanced Geothermal Systems: Modelling Heat and Mass Transfer in Fractured Crystalline Rock

Kaiu Piipponen
2017

Advisor:	Ilmo Kukkonen
Examiners:	Ilmo Kukkonen
	David Whipp

UNIVERSITY OF HELSINKI
DEPARTMENT OF PHYSICS

PL 64 (Gustaf Hällströmin katu 2)
00014 University of Helsinki

HELSINGIN YLIOPISTO — HELSINGFORS UNIVERSITET — UNIVERSITY OF HELSINKI

Tiedekunta/Osasto — Fakultet/Sektion — Faculty	Laitos — Institution — Department
Faculty of Science	Department of Physics

Tekijä — Författare — Author
Kaiu Piipponen

Työn nimi — Arbetets titel — Title

Enhanced Geothermal Systems: Modelling Heat and Mass Transfer in Fractured Crystalline Rock

Oppiaine — Läroämne — Subject
Sold Earth Geophysics

Työn laji — Arbetets art — Level	Aika — Datum — Month and year	Sivumäärä — Sidoantal — Number of pages
Master's thesis	October 2017	61

Tiivistelmä — Referat — Abstract

Geothermal energy is a growing industry and with Enhanced Geothermal System (EGS) technology it is possible to utilize geothermal energy in low heat flow areas. The ongoing EGS project in Southern Finland provides a great opportunity to learn and explore EGS technologies in a complex environment: hard crystalline rock, high pressure and low hydraulic permeability. This work describes physics behind an EGS plant, as well as basic concept of EGS, give examples of some existing plants and make calculations of how much power a plant in Finland can produce. In order to plan and build a successful plant, suitable parameters for the system are determined by modelling. The modelling is done analytically and numerically.

Physical properties governing the EGS models are conductive and convective heat transfer and rock hydraulic properties that allow fluid flow. Hydraulic permeability is discussed in detail, because it is the key parameter in EGS: rock is stimulated in order to enhance permeability in order to make fluid flow possible through interconnected fractures. It is a spatially correlated parameter and it is distributed lognormally making fluid flow highly channelled.

Modelling of heat and mass transfer aims to parametrize an EGS plant in the conditions of Southern Finland. The parameters governing heat transfer with fluid flowing in the geothermal reservoir are size of the reservoir and fluid velocity, which depends on matrix permeability. The larger the reservoir the more hot contact area fluid encounters and the better it heats up, the slower the flow, the longer time fluid stays in the reservoir and therefore heats up more. High flow rates cool the reservoir rapidly. However, a large reservoir is difficult to achieve, maintaining enhanced permeability requires relatively high fluid flow rates and the higher the flow rate, the more power the plant produces, so slow flow is not economically feasible.

Analytical models are done with Matlab and numerical models are done with finite-element software COMSOL Multiphysics. Numerical models benchmark the analytical solutions and use spatially correlated permeability to modify fluid flow pattern and see how temperature in the reservoir changes with changes in fluid flow.

The results show that creating large reservoir that could operate for 20 years with desired power production is unrealistic. Total output fluid flow required to produce over 1 MW of power is 10 kg/s. At such rate there is a risk that the reservoir cools and output fluid temperature is not sufficient for power production. In case of heterogeneous permeability connectivity of the reservoir is not as good as in case of homogeneous permeability and there is a risk that total fluid flow in the reservoir is slower and therefore less power produced.

Avainsanat — Nyckelord — Keywords
EGS, geothermal modelling, hydraulic permeability, COMSOL Multiphysics

Säilytyspaikka — Förvaringsställe — Where deposited
Kumpula campus library

Muita tietoja — Övriga uppgifter — Additional information

Contents

Kiitokset

Suuret kiitokset tämän lopputyön toteutumisesta kuuluvat ohjaajalleni professori Ilmo Kukkoselle, joka kärsivällisesti mahdollisti työni aiheen parissa, ohjasi minut geotermiikan maailmaan sekä antoi arvokkaita kontakteja. Kiitos gradun toiselle tarkastajalle David Whippille. Erittäin arvokasta keskustelua kävin Pekka Malinin sekä Peter Learyn kanssa, joilta sain myös koodin mallini poroperm-jakaumaan.

Opiskeluvuoteni Helsingin yliopistossa ovat olleet tapahtumarikasta aikaa. Ystävät istuutuivat pöydän ääreen kuuntelemaan, kun olin menettää uskon tekemisiini, ja löivät bambukepillä, kun en jaksanut eteenpäin. Opiskeluaika ei ollut ainoastaan kurssien puurtamista, mistä pitivät huolen rakkaat ainejärjestöni Geysir ry. ja Resonanssi ry. Noora ja Piri ovat pysyneet rinnallani fuksista saakka, ja muut kanssaopiskelijat ovat tarjonneet vähintään yhtä arvokasta vertaistukea.

Äitini mahdollisti elämäni ja koulutukseni Suomessa ja on aina tukenut minua valinnoissani. Isä istutti kiinnostuksen kiviin viemällä mineraalikabinetteihin jo ennen kouluikää.

Kiitos myös Jerelle, ihan kaikesta.

List of symbols

Latin symbols

A	Radiogenic heat production (W/m^3)
a	Empirical constant of poroperm relation
b	Fracture width (m)
c	Specific heat capacity (J/kg K)
d	Characteristic length (m)
F	Mass transfer rate (kg/s)
g	Gravitational acceleration (m/s^2)
h	Fracture aperture (m)
K	Hydraulic conductivity (m/s)
k	Spatial frequency of Fourier power spectrum
L	Distance between wells (m)
Pe	Peclet number
Q	Heat flow density (W/m^2)
q	Fluid flow rate (m/s or m^3/m^{2}s)
R	Radius of the fracture (m)
Re	Reynolds number
S	Fourier power spectrum
T	Temperature (K)

t Time (s)

u Fluid velocity (m/s or m^3/m^2s)

V Volume (m^3)

Greek symbols

α Diffusivity (m^2)

β Scaling parameter of Fourier power spectrum

κ Permeability tensor (m^2)

Λ Flow geometry factor

λ Thermal conductivity (W/K m s)

μ Fluid viscosity (Pa s)

ϕ Porosity

ρ Density (kg/m^3)

σ Stress (Pa s)

τ Shear stress (Pa s)

θ Streamline

φ Angle of internal friction

ξ Equipotential line

Subscripts

i Initial

p Pore pressure (in stress notation)

r Rock

v Vertical (in stress notation)

w Fluid

Chapter 1

Introduction

Geothermal energy provides a renewable source of energy for electricity production and space heating with low greenhouse gas emissions and is therefore an important addition to the energy market, which is nowadays strongly dominated by fossil fuels. Heat in the crust and mantle originates from planetary accretion processes and heat production by decay of radioactive isotopes of mainly ^{40}K, ^{232}Th, ^{235}U and ^{238}U (Turcotte and Schubert, 2002). The outflow of heat to the surface of the Earth is controlled by various tectonic processes and therefore global distribution of heat flux is not uniform. This heat can be exploited for direct use or electricity generation, and possible utilisation depends largely on areal heat flow.

Geothermal energy accounted for 0.4% of world's energy supply in 2015 (Figure 1.1) (IEA, 2017). The percentage is very small considering the enormous potential - Intergovernmental Panel on Climate Change (IPCC) estimates geothermal energy potential to be from 10 to 312 EJ/a (10^{18}J/a) while the use of this potential is estimated to be 0.24 - 0.41 EJ/a (Goldstein et al., 2011), meaning that 0.1 - 2 % of estimated potential is actually utilised. While production of geothermal energy has nearly doubled between years 1990 and 2015, its increase has still been small and concentrated mainly to OECD countries with the largest single producer being USA (IEA, 2017, Lund, 2007). What makes deployment of geothermal energy challenging is

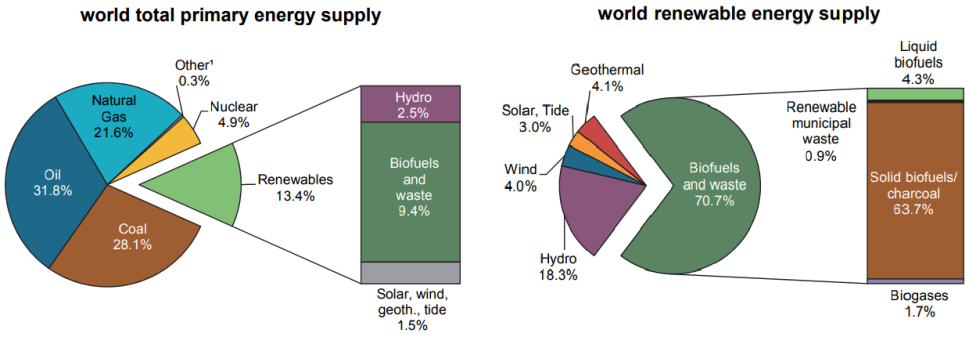

Figure 1.1: Worldwide energy supply in 2015, Source: IEA (2017)

the uneven distribution of areas with high surface heat flow as well as the related geological and technological challenges.

Areas near lithospheric plate boundaries or at hot spot anomalies have a long history of using geothermally heated water for various purposes. Utilization depends on temperature of the extracted fluid, and examples of possible ways to use geothermal fluids are listed in the Líndal diagram in Figure 1.2. "General industry" of the diagram includes different agriculture, such as animal husbandry, mushroom growing, drying farm products or timber, extraction of salts by evaporation, refrigeration and alumina industry (Líndal, 1973). The diagram also lists temperature ranges for geothermal energy used for electricity production and heating. Space heating and cooling is the main utilization of geothermal energy due to its small scale and wide availability (Fridleifsson, 1998). Heat pump systems do not require high temperature to operate, and therefore production cost is low.

On the high temperature end of the Líndal diagram is "power production" which operates at temperatures high enough to use steam condensing turbines and binary cycle units (Goldstein et al., 2011). Subsurface fluids of temperature over 150°C are circulated in the power plant so that vapour runs through the turbine and condensed hot water is further utilized for direct use. Binary plants are used in hot water dominated reservoirs by employing substances with a lower boiling point to drive turbines. Two most commonly used binary plant systems are Organic Rankine Cycle (ORC) and Kalina Cy-

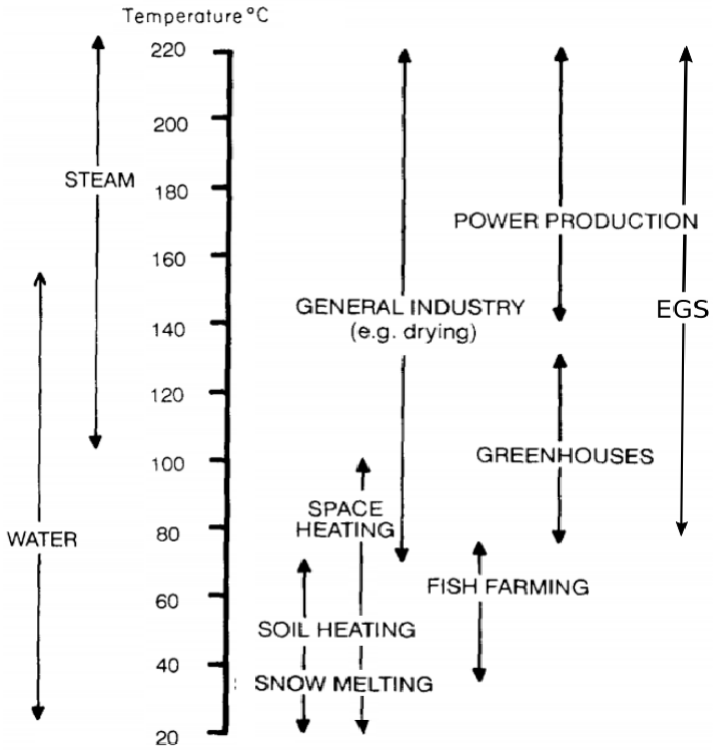

Figure 1.2: Utilization of geothermal energy at different temperatures, (Adapted from Líndal (1973) and Armansson and Kristmannsdóttir (1992))

cle, that use different working fluids. New innovations provide possibilities to deploy fluids of supercritical temperatures (>374 °C). (Goldstein et al., 2011; Arriaga and Samaniego, 2012)

Conventional hydrothermal systems are limited to the sparse areas of high heat flow. There is potential for large scale geothermal energy production outside high heat flow areas, especially considering large demand of energy for space heating and cooling, which does not require fluid temperatures as high as electricity generation. These geothermal plants must reach deeper in order to achieve high temperatures or alternatively use heat pumps to increase the temperature to the desired level. The fluid circulation through the reservoir does not occur naturally but has to be created and maintained artificially, as well as good hydraulic permeability of the reservoir. Such geothermal plants are called Hot Dry Rock (HDR) or Enhanced Geothermal Systems (EGS).

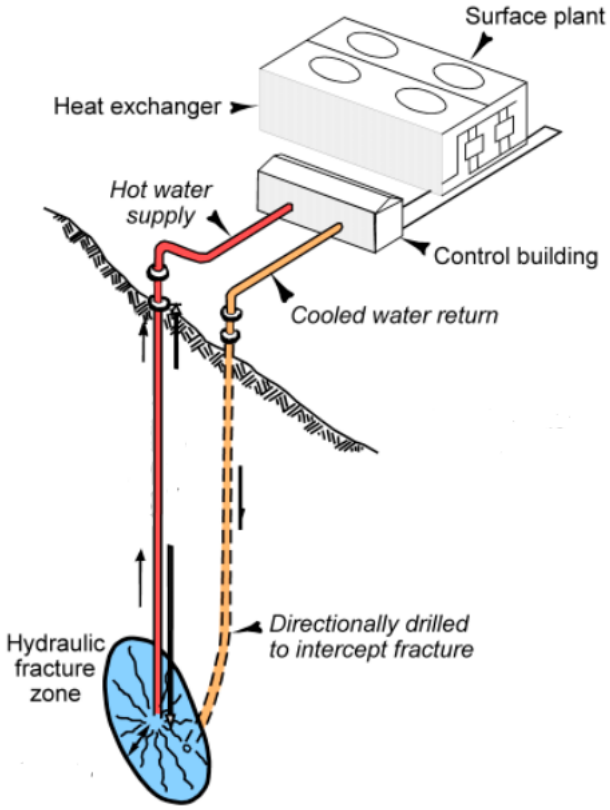

Figure 1.3: Concept of an HDR/EGS plant (From Lund (2007))

1.1 Aim and contents of this thesis

The Enhanced geothermal system (EGS) projects are ongoing in several countries, including Southern Finland. The current work is motivated by the currently increasing interest towards EGS systems in crystalline rocks in general and the currently (2015-2018) running pilot project in Espoo, Southern Finland. The project aims to drill to 6-7 km depth and to construct an EGS plant to produce heat energy for district heating in Espoo area. Conditions for EGS in Southern Finland are challenging, because due to low geothermal gradient achieving hot enough rock (>100°C) requires drilling to 6 km or deeper. At such depths high pressure and low fluid permeability make the reservoir development difficult. Rock hydraulic permeability must be enhanced in order to increase fluid flow to transfer the subsurface heat.

Modelling flow conditions in the subsurface is done in order to obtain feasible parameters required for successful fluid circulation. Finding these parameters helps in developing a properly functioning geothermal heat plant.

The aim of this thesis is to give an insight to EGS from a geophysical perspective and describe analytical and numerical models that can be modified for application in different geothermal regimes. This work is divided into three chapters.

Chapter 2 studies the physical background of the involved phenomena: heat transport, fluid flow, hydraulic properties of rock and relevant rock mechanics. Basic equations of conservation of thermal energy and mass are presented and permeability is discussed in greater detail. Permeability is a complex parameter and the most important factor to be stimulated before and during production. It is accounted as a spatially correlated parameter with log-normal distribution. Rock mechanics determines how fractures form and open when rock is stimulated, so it is crucial to know the state of stress of the planned production area in order to be able to enhance the hydraulic permeability of the reservoir.

Chapter 3 covers the principles of EGS, briefly discusses drilling and permeability enhancement methods and describes some existing EGS plants. Estimation of possible energy production is discussed and calculated. It is also important to take a look at the sustainability of production and possible environmental impacts an EGS plant may have. While the system has no direct CO_2 emissions and many other environmental impacts are smaller than for example with the hydrothermal plants, drilling and utilizing subsurface heat has some consequences to the environment, such as seismic hazard and waste water treatment.

Chapter 4 presents both analytical and numerical models for heat and mass transfer within the reservoir in cases of homogeneous and heterogeneous permeability models applied. The analytical model applied here is based on solutions of equations of heat and mass transfer provided by Rodemann (1979). The numerical models were calculated with COMSOL Multiphysics

finite element analysis software. Two different approaches complement each other. Numerical models also demonstrate the role of permeability distribution during production.

These chapters are followed by discussion and conclusions. The developed models are simple and robust, so they can be applied to any area to parametrize the system. The final chapter presents some alternatives and an outlook how the EGS in crystalline rock could be utilized in order to improve the system.

Chapter 2

Physical background

Physical factors relevant to subsurface heat transfer and fluid flow are heat transfer (section 2.1), fluid flow (section 2.2), hydraulic properties of the crystalline rock (section 2.3) and mechanical behaviour of the rock and stress field (section 2.4).

The main problem discussed in this thesis is the thermal and fluid flow regime in a geothermal reservoir, where heat transfer with conduction and convection must be balanced in order to maintain temperature of the rock at high enough level for the reservoir to stay productive for a required time. It is apparent that the deeper inside the crust we drill, the hotter it is, but simultaneously lithostatic pressure increases resulting in closure of pores and fractures. This leads to reduction of fluid circulation and technical difficulties in drilling and permeability engineering.

The most important parameter governing fluid transport is hydraulic permeability. Fluid flow depends on how well fractures are interconnected, and in order to increase flow this connectivity needs to be enhanced. It is important to determine the orientation of the fracture systems in order to be able to properly enhance reservoir permeability. Fractures striking perpendicularly to the least principal stress component open first, and such structures are the most potential targets for hydraulic stimulation Therefore, the knowledge of the local stress field is important, and it controls whether the stimulation is

able to connect and widen the existing fractures.

First law of thermodynamics states that the same amount of thermal energy and mass that enter the system must leave the system. The conservation laws of thermal energy and mass are summarized by continuity equations for heat and fluid flow:

$$\rho c \frac{\delta T}{\delta t} + \nabla \cdot \mathbf{q} = 0 \tag{2.1}$$

and

$$\frac{\delta \rho}{\delta t} + \nabla \cdot (\rho \mathbf{u}) = 0 \tag{2.2}$$

where ρ is density of matter transferring heat or density fluid, respectively, c is specific heat capacity at constant pressure, T temperature, q heat flux vector (transfer of heat per unit cross-sectional area per unit time) and u fluid flow velocity vector. For incompressible fluids (ρ is constant) equation 2.2 simplifies to

$$\nabla \cdot \mathbf{u} = 0 \tag{2.3}$$

2.1 Heat transfer

Natural heat transfer in the lithosphere occurs mostly by conduction. Convection is less important on a crustal scale, but local fluid flow may disturb the conductive heat flow. Heat transfer by radiation is not relevant in the lithosphere in normal conditions, because radiation requires transparency. The law of conservation of energy (Equation 2.1) governs heat transfer.

2.1.1 Conduction

Heat flow density Q is defined as a product of thermal conductivity of the rock (λ) and temperature gradient. This is Fourier's first law of heat conduction:

$$Q = -\lambda \frac{\delta T}{\delta z} \tag{2.4}$$

The net change in temperature of the body depends on net heat flow through the volume, properties of the material and heat generation in the volume. (Carslaw and Jaeger, 1959)

In unit time one-dimensional change in temperature is expressed as

$$c\rho \frac{\delta T}{\delta t} = -\frac{\delta Q}{\delta z} + A, \tag{2.5}$$

where A is net heat production. Heat generation includes radiogenic heat production, tectonic and volcanic processes and tidal heating (Ledru and Frottier, 2010). Combining equations 2.4 and 2.5 and expanding heat flow to apply in three dimensions,

$$c\rho \frac{\delta T}{\delta t} = -\lambda \nabla^2 T + A, \quad \alpha = \frac{\lambda}{c\rho}$$

so

$$\frac{\delta T}{\delta t} = \alpha \nabla^2 T + \frac{A}{c\rho}, \tag{2.6}$$

where α is thermal diffusivity, a function of λ, c and ρ. This equation describes conductive heat flow in an isotropic medium. With no heat production equation 2.6 simplifies to diffusion equation:

$$\frac{\delta T}{\delta t} = \alpha \nabla^2 T, \tag{2.7}$$

2.1.2 Convection

Heat transfer occurs with motion of either pore filling fluid or the medium. It can be fluid flowing through pores and fractures as well as erosion or deposition that causes change in the distance between observed volume and surface of fixed temperature. Advective transfer term is added to Equation 2.6 and it takes form

$$\frac{\delta T}{\delta t} = \alpha \nabla^2 T + \frac{A}{c\rho} - \mathbf{u} \cdot \nabla T \tag{2.8}$$

where $\mathbf{u}$ is fluid velocity (Fowler, 2005). Equation 2.8 and its solutions provided by Bodvarsson (1969) and Rodemann (1979) are the fundamental equations used in this thesis, Chapter 4.

The ratio of heat transferred by convection and conduction is a dimensionless *Péclet number* (Pe). When $Pe > 1$ heat flow is convection dominated, when $Pe < 1$ heat flow is dominated by conduction.

$$Pe = \frac{convection}{conduction} = \frac{\mathbf{u}d}{\alpha} \tag{2.9}$$

where d is a characteristic length, that may be, for example, thickness of the studied layer or wellbore radius. In porous matric convective numerator includes porosity ϕ.

2.2 Fluid flow

At small depths pores and fractures are filled with fluid, mainly water with salts dissolved in it. Subsurface motion is caused by changes in hydrostatic pressure or hydraulic (piezometric) head, the sum of pressure head and elevation head. Pressure head is the "pressure energy per unit weight of fluid", or the height of the water column measured from the bottom of piezometer. (Bear, 1973)

Fluid flow in porous medium follows conservation of mass (Equation 2.2) and is described by Darcy's law. Specific discharge q per unit area is a function of hydraulic permeability of the rock, viscosity of the fluid and pressure gradient. In three-dimensional form Darcy's law also takes into account gravity:

$$\mathbf{q} = \frac{\kappa}{\mu}(\nabla p - \rho \mathbf{g}) \qquad \text{and} \qquad \mathbf{q} = \frac{\kappa}{\mu}\frac{\delta p}{\delta x} \tag{2.10}$$

where κ is permeability tensor, μ and ρ are viscosity and density of fluid respectively, g acceleration due to gravity and ∇p is pressure gradient.

The flow takes place only in intergranular space, so velocity of fluid is defined as the average flux per porosity of matrix:

$$\mathbf{u} = \frac{\mathbf{q}}{\phi}$$

where $\mathbf{u}$ is fluid velocity vector in the matrix and ϕ is porosity. (Whitaker, 1986)

Important limitation of Darcy's law is that it is only valid at laminar flow velocities. To distinguish between laminar and turbulent flow in a conduit the ratio of inertial to viscous forces is studied. The ratio is called *Reynolds number* (Re) and the critical value between laminar and turbulent flow is $Re = 2100$. Reynolds number for porous media is defined as

$$Re = \frac{q\rho d}{\mu} \tag{2.11}$$

where d is a value related to grain size distribution, a *representative grain diameter*. Empirically defined transition to non-Darcian flow takes place already at $Re \sim 5$. Velocities high enough for turbulent flow are rare in the subsurface, sometimes occurring near wellbores. (Bear, 1973; Ingebritsen et al., 2008)

2.3 Permeability and porosity

As mentioned in a previous section 2.2, permeability is an important and complex parameter that defines how fluid flows in the subsurface. Often permeability and porosity are mistakenly used interchangeably, but in reality the correlation varies largely with rocks. Porosity is a percentage of void space within the rock matrix, typically filled with fluid at subsurface below groundwater table. Whereas porosity is high in sedimentary rocks, in crystalline rock it is very low (< 0.01) and consists mainly of fractures within the rock. Permeability describes how freely fluid can move within the fractures or pores. Even a very porous rock matrix may have small permeability if its pores are not interconnected.

If flow and pressure gradients are known, simple estimate on average

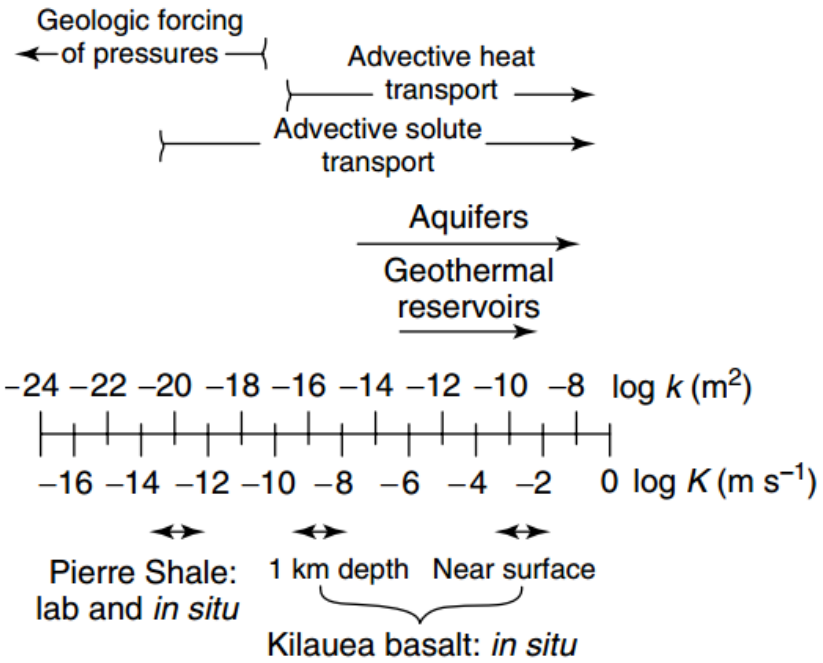

Figure 2.1: Ranges of permeabilities (k) and hydraulic conductivities (K) observed in geologic media in relation to water density and viscosity at 15°C. From Ledru and Frottier (2010)

permeability can be calculated from Darcy's law (Equation 2.10):

$$\kappa = \frac{\mu q}{\nabla p} \tag{2.12}$$

The calculation can be used in a laboratory conditions to measure permeability. However, average permeability is only a directional parameter for a certain rock type of certain porosity at certain pressure (Figure 2.1). Permeability is an anisotropic parameter, so direction of fractures plays role when measuring porosity in the laboratory. Due to the heterogenous and anisotropic nature of the parameter, it is difficult to find representative samples to define permeability. Ingebritsen et al. (2008) suggest 10^3-fold variations of permeability in crystalline rock.

Large space and time scales present in many geologic problems make it particularly complicated to define permeability. Depth dependency is shown with increase in confining pressure and effective stress that cause a decrease in porosity and closure of fractures. Ingebritsen and Manning (1999) present a permeability-depth relation model as an empirical power-law fit for different permeability data:

$$\log \kappa \approx -14 - 3.2 \log z \tag{2.13}$$

where κ is permeability in m^2 and z depth in km. This model only describes crustal scale permeability and does not take into account local variations. It shows a rapid decrease in permeability with depth. The model takes into consideration the brittle-ductile transition regime at 10-15 km depth and sets permeability below it at constant value of $\log \kappa = 18.3$. Permeability-depth curves are presented in Figure 2.2.

Crystalline rock has heterogeneous rheology and permeability concentrates to narrow regions that can be lithologic units or fractures. This type of flow is called channeled (Manning and Ingebritsen, 1999). Rock permeability varies spatially, and if the fracture system is connected, the fractures open

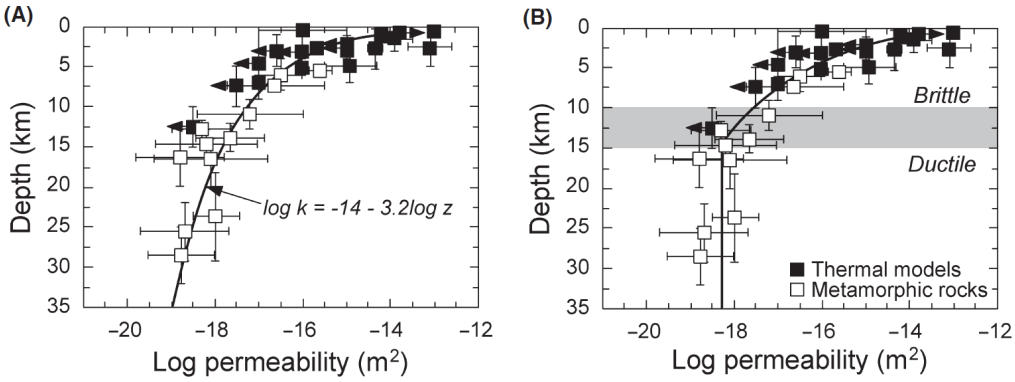

Figure 2.2: Permeability-depth curves for A) power-law fit to data and B) depths below BDT with constant $\kappa = 10^{18.3}$ m^2. From Ingebritsen and Manning (1999)

further when stimulated with hydraulic overpressure. Most of the crystalline rock has very low permeability and fractures account for only a fraction of volume within the rock. However, fluid flows mainly through this fraction.

2.3.1 Flow lognormality and spatial correlations in crustal reservoirs

The average permeability formulation assumes crustal properties to be normally distributed and uncorrelated and that they can therefore be averaged. Averaging simplifies computation, but the results do not correlate with reality. If permeability is spatially correlated, as empirical observations show, instead of averaging, spatial fluctuation should be included in calculation.

Fracture distribution in crystalline rock can be quantified following statistical rules. In the tripartite publication "Flow Lognormality & Spatial Correlation in Crustal Reservoirs" Leary et al., Malin et al. and Pogacnik et al. describe three empirical properties that have been observed to apply to crustal reservoirs world-wide:

- Spatial correlation of different scales that can be seen in power-law spectra of spatial correlation of a well-log

- Correlation of fracture density and fracture connectivity on a grain scale, seen as correlation of porosity and permeability in a well-core
- Correlation of porosity and permeability on a reservoir scale.

These empirics concentrate on the granular nature of the rock rather than spatially-averaged effective continuum.

The first rule is for spatial correlation: "the degree of spatial fluctuation power of *in situ* rock properties increases linearly with the scale on which the spatial fluctuation power is measured" (Malin et al., 2015). There is tendency that crustal volume elements have similar properties than neighbouring volume elements of the same scale.
Mathematically the rule is expressed as

$$S(k) \propto \frac{1}{k^{\beta}}, \quad \beta \approx 1 \tag{2.14}$$

where S is the Fourier power-spectrum and k spatial frequency of a scale $1/cm < k < 1/km$. β is a scaling parameter that defines the grade of correlation. The larger k is, the larger are the deviations from mean background value.

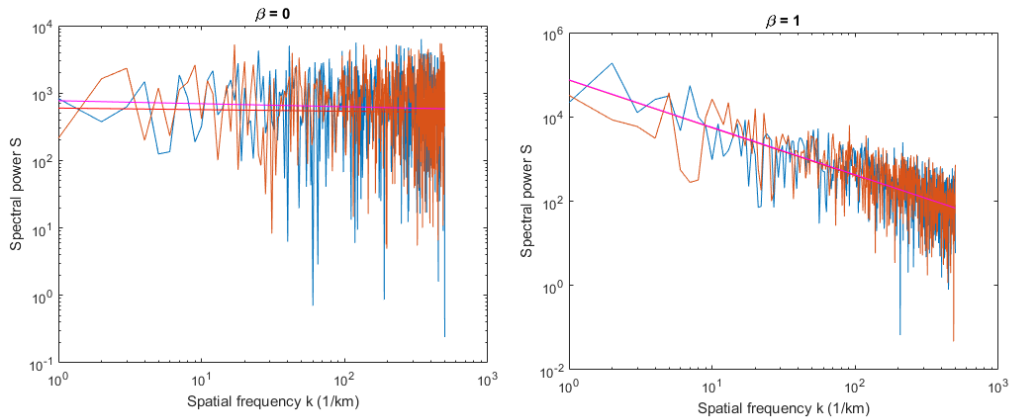

Figure 2.3: Spectral power-logs as function of k with different degrees of correlation. When $\beta = 0$, S stays relatively uniform across the spatial frequency scale and when $\beta = 1$, S decreases with k

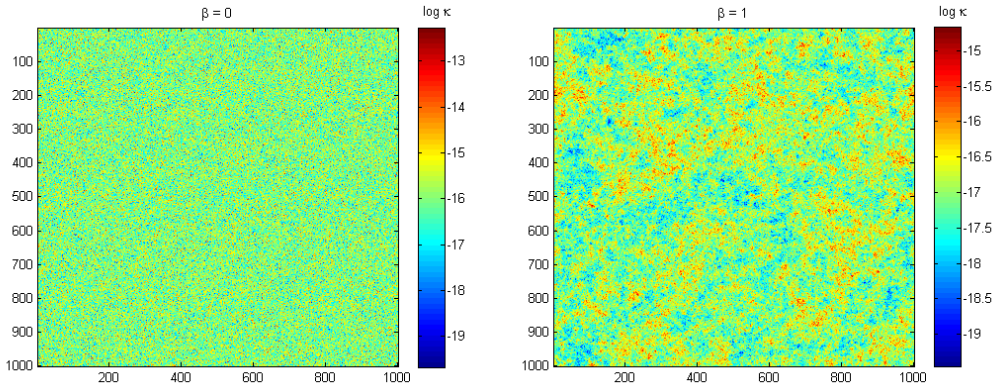

Figure 2.4: When $\beta = 0$, 2D permeability distribution is homogeneous white noise with no correlation. With $\beta = 1$ permeability distribution is at higher degree of spatial correlation.

The expression is visualised in Figures 2.3-2.4 showing the difference between $\beta = 0$ and $\beta \approx 1$. $\beta = 0$ gives white noise, whereas the higher β the higher degree of spatial correlation: points next to each other tend to have similar values on a same scale and they form networks.

The second rule creates a correlation between porosity fluctuations and permeability fluctuations. It has been observed in well-core measurements that fluctuations in core porosity cause fluctuations in the logarithm of core permeability:

$$\delta\phi \propto \delta \log(\kappa), \tag{2.15}$$

The third rule is in integration of rule 2 from a scale of centimeters to kilometers:

$$\kappa \propto \exp(a\phi), \tag{2.16}$$

Observed values for a dimensionless integration constant a are typically 30-50 for formation porosities of 0.1-0.3. When porosity ϕ has fixed normal distribution, distribution of κ depends on the integration constant a: small a returns normal distribution while a larger vslue of a returns more log-normal

distributions (Figure 2.5). In case of porosity as low as in crystalline rock ($\phi \approx 0.01$) a would be $300-500$ in order to maintain log-normal permeability distribution, so that $a\phi \approx 5$. This is physically interpreted as the degree of fluid flow controlled by fracture connectivity - in other words the above mentioned channelled flow.

Lognormal permeability distributions are observed worldwide in conventional and unconventional oil and gas fields, nuclear waste deposition sites, groundwater aquifers and geothermal fields (Leary et al., 2017; Leary and Al-Kindy, 2002).

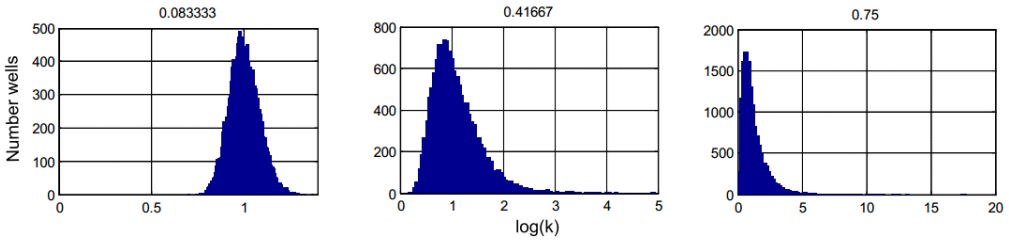

Figure 2.5: Progression from normal distributions to lognormal distributions of permeability as a function of empirical integration parameter a for a fixed distribution of porosity. Values of $a < 10$ give nearly normal permeability distributions, values of a in range $30 < a < 60$ give increasingly lognormal permeability distributions widely observed in reservoirs. (Pogacnik et al., 2015)

2.4 Rock mechanics

Enhancing permeability is done by stimulating pre-existing fractures. Stress distribution dictates the minimum pressure in order to widen and extend the existing fractures. The orientation of the stimulated fractures depends on stress tensor: depending on the direction of minimum stress the fracture system will be horizontal or vertical. Rock mechanics is a versatile field of study by itself and this section aims to briefly discuss areas relevant to EGS.

Regional stress field is determined from lithospheric stress models, regional geological observations, such as faults, and indicators appearing during drilling, such as failure along borehole walls and drilling-induced tensile fractures. It can also be determined with several active methods, such as hy-

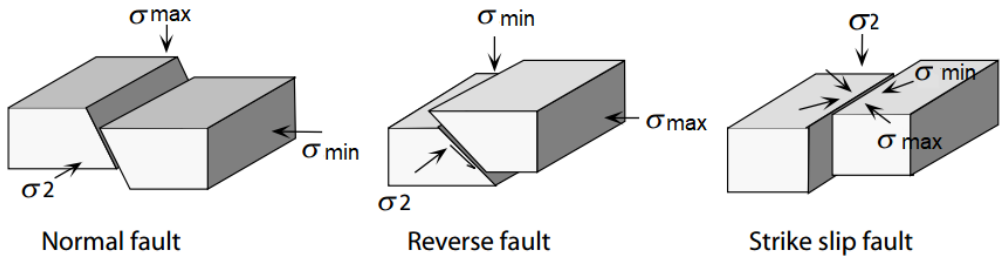

Figure 2.6: Three faulting environments and associated stress components, $\sigma_{max} > \sigma_2 > \sigma_{min}$. Adapted from Stüwe (2007)

draulic fracturing or overcoring (Bruhn et al., 2010; Ljunggren et al., 2003). Subsurface stress regime is dictated by a stress tensor that can be simplified to use only the three principal stresses σ_1, σ_2 and σ_3. As a general rule within a relatively uniform topography one principal stress direction is (nearly) vertical and two are (nearly) horizontal, so $\sigma_3 = \sigma_v$ is the vertical component (Anderson, 1951). It is dictated by density and thickness of each layer of overlying rock:

$$\sigma_v = \Sigma_{i=1}^{n} \rho_i g z_i \tag{2.17}$$

Since variation in σ_v is small, the different faulting environments are associated with changes in two horizontal stress components and their relation to the vertical component. Possible faulting environments of frictional faulting theory of Anderson are normal faulting, strike-slip faulting and thrust/reverse faulting (Figure 2.6). Assuming that vertical stress has a constant value (Equation 2.17), in case of normal faulting there occurs relaxation of both horizontal stresses and σ_v is the largest component, in case of strike-slip faulting one horizontal stress component increases while another decreases, so $\sigma_1 > \sigma_v > \sigma_2$ and in case of thrust faulting both horizontal stress components are larger than vertical stress component. The three faulting environments are visualized in Figure 2.6.

Combining the methods to determine the stress regime and evaluating

the vertical stress, the complete stress tensor can be calculated:

$$\sigma_{tot} = \begin{pmatrix} \sigma_{xx} & \tau_{xy} & \tau_{xz} \\ \tau_{xy} & \sigma_{yy} & \tau_{yz} \\ \tau_{zx} & \sigma_{zy} & \sigma_{zz} \end{pmatrix} \tag{2.18}$$

where τ are the shear stress components. The failure mode is dependent on differential stress $\sigma_1 - \sigma_3$: near the surface at low differential stress the failure mode is tensile and at high differential stress shear failure is more likely to occur (Bruhn et al., 2010).

Pore pressure plays significant role in lowering the strength of the lithosphere. In the absence of any processes pore pressure is hydrostatic, but tectonics, heating, dehydration of minerals or fluid injection cause changes in pore pressure. Increased formation pressure decreases normal stress acting on planes:

$$\sigma = \sigma_{tot} - \sigma_p \tag{2.19}$$

where σ_{tot} is a normal component and σ_p pore pressure. According to the Mohr-Coulomb criterion slip along a plane in the rock occurs when the shear stress along that plane reaches the critical value:

$$\tau_{crit} = \tau_0 + \sigma \tan \varphi \tag{2.20}$$

where φ is the angle of internal friction. When fracture is initiated, τ_0, the shear strength, is eliminated, and pore pressure decreases stress required for failure:

$$\tau_{crit} = (\sigma_{tot} - \sigma_p) \tan \varphi \tag{2.21}$$

Hubbert and Rubey (1959) suggest that with very high pore pressures even large blocks of rock can be displaced at low angles. Hydrofrac stim-

ulation used to enhance permeability increases pore pressure and modifies *in-situ* stress distribution, sometimes so much it may change fault behavior (Schulte et al., 2010).

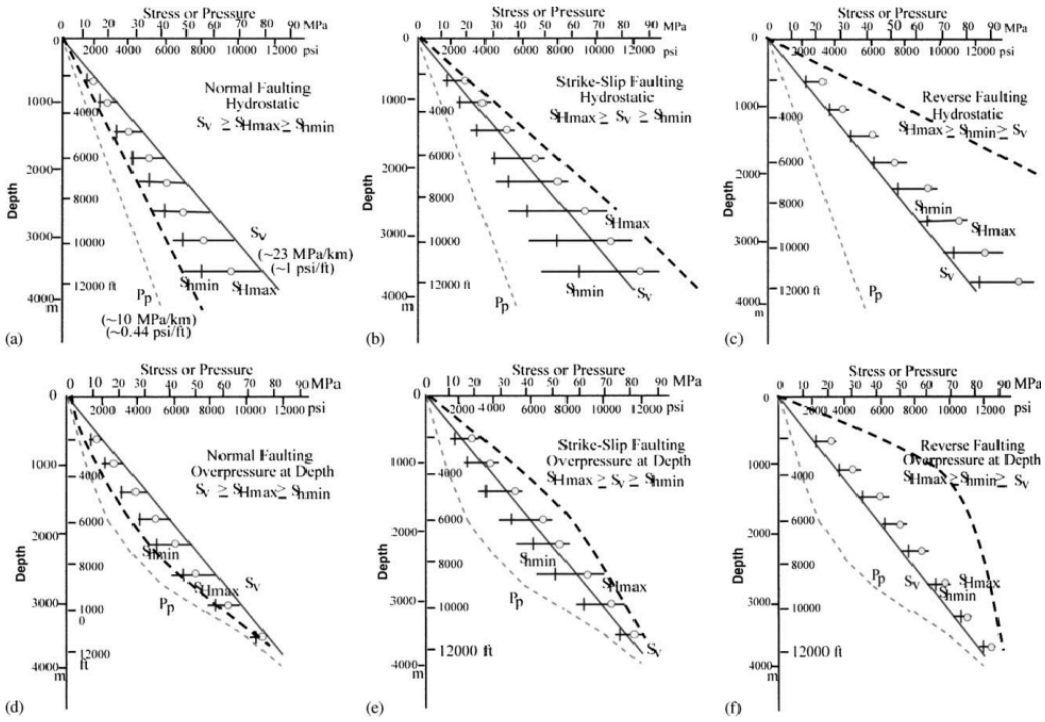

Figure 2.7: Variation of stress magnitudes with depth in normal, strike-slip and reverse fault stress regimes for hydrostatic (a–c) and overpressure conditions (d–f). The heavy dashed lines indicate the limiting case for stress magnitudes based on frictional faulting theory. From Zoback et al., 2003

The relations of magnitudes of deviatoric stress (the difference between minimum and maximum stress), pore pressure and strength of the lithosphere are summarized in Figure 2.7. The difference between σ_{min} and σ_{max} increases with depth due to increase of crustal strength with depth. However, the difference decreases in case of overpressure due to the decrease of crustal strength with elevated pore pressure. In cases of overpressure, three principal stresses are very close to each other in each of the faulting regimes.

Disturbances in stress field may induce perceptible seismicity, which is often a public concern.

Another issue related to the stress regime is borehole stability. It depends on faulting environment. Stress on borehole wall is divided into axial, radial and tangential stresses. One way to stabilize borehole during drilling is to use very viscous high-density drilling mud. The function of drilling mud is to cool the drill bit, transport the drill cuttings upwards, reduce friction, stabilize the borehole wall and exert pressure on borehole walls in order to prevent formation fluids from entering the borehole. When borehole is very stable and rock is dry, air can be used as a drilling fluid, otherwise the drilling mud is water or oil based. Water is used most commonly, but different additives are added to improve characteristics: barite to increase density, polymers to reduce friction and improve rheology, foaming agents to avoid mud from filtrating to porous formations. (Sperber et al., 2010)

Chapter 3

Enhanced Geothermal System

In order to make energy production feasible in low porosity crystalline rock, different methods than conventional hydrothermal plants must be used. If no natural hydrothermal circulation occurs at the site the reservoir is created artificially: permeability is engineered to be sufficiently high and water is circulated with pumps. The system needs a large reservoir: the more heat exchange surface the circulating fluid encounters, the more efficient heat extraction is. Hot Dry Rock (HDR) systems rely on discrete hydraulic fracturing that creates a large enough surface for heat transfer from rock to fluid, whereas aim of Enhanced/Engineered Geothermal System (EGS) is to stimulate a natural fracture system. EGS is a newer term and some EGS projects are accounted as HDR in older literature.

EGS plants vary with design in each location depending on rock properties, but the concept is to have a fracture network between injection and production wells, as demonstrated in Figure 3.1. Depending on the in situ stress fractures propagate horizontally or vertically, and wells must be drilled directionally so that created fracture network connects injection and production wells.

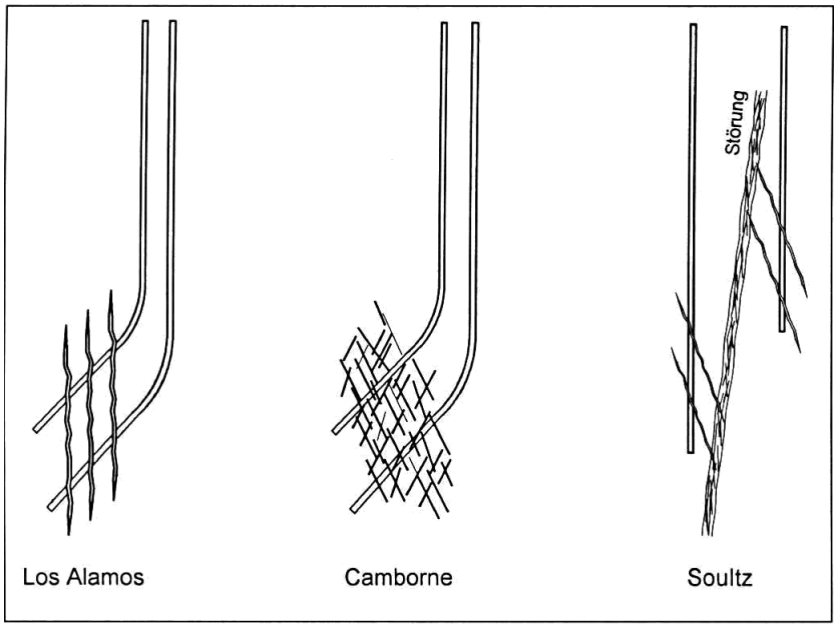

Figure 3.1: Examples of possible fracture networks in EGS principle, from Tenzer (2001)

3.1 Enhancing permeability

Permeability stimulation is done mechanically by injecting large amounts of fluid at high pressure in the wells or chemically by dissolving minerals that are sealing natural fractures. Hydraulic stimulation is known from hydrocarbon industry. In geothermal reservoirs the application requires large amounts of fluid. Waterfrac treatments produce long fractures with small apertures. The efficiency depends on potential shear displacement and how sheared rock mass maintains the fracture by itself. Gel can be used as a proppant instead of water, or both can be used in so-called hybrid fracturing. Injection fluid is often cold in order to cause thermal stress in a hot rock mass. The cooling rock matrix contracts and induces a tensile component of subsurface stress, thermoelastic stress. (Schulte et al., 2010)

Chemical stimulation is done mainly in sandstones by aciziding rock matrix in near-wellbore region. It is most efficient at removing siliceous particles of drilling mud and restoring permeability. Used acids are hydrochloric acid

(HCl) and hydrofluoric acid (HF) - former to treat limestone, dolomite, and calcareous areas, latter to dissolve clay minerals and silica. (Schulte et al., 2010)

Enhancing permeability by increasing the injection pressure has some negative throwbacks: pushing the existing fractures allows few flow paths to dominate the flow and short circuits occur, and if critical pressure of fracture growth occurs, the reservoir might extend and allow water to escape the circulating system. (Tester et al., 2006)

Such dispersion of pore fluids allows fractures close (and eventually heal) to densities below critical. This suggests that in order to maintain fractures pore pressure must be near lithostatic. (Crampin, 1994)

3.2 Examples of EGS around the world

Geothermal energy production in crystalline rock has been under development worldwide. There are operating or experimental plants in the US, Australia, Japan and several European countries, including UK, France, Germany and Switzerland (Tester et al., 2006).

3.2.1 Fenton Hill

The first "man-made" geothermal reservoir was created in Los Alamos National Laboratory in Fenton Hill, New Mexico, USA. The project was run from 1972 to 1996. The test site was located west of the 1.26 Ma old Valles Caldera, in the proximity to recent volcanic activity so the Precambrian basement rock was influenced by heat and pore fluid radially diffusing from the caldera. Geothermal gradient of overlying Paleozoic sediments is over 100 °C/km and around 50 °C/km in the basement. (Brown et al., 2012)

Two reservoirs were created, Phase I was at depth of 2800-2950 m (180-200 °C) and Phase II at 3500 m (240 °C). Phase I reservoir was enlarged in stages, work beginning in 1974 and finally after several attempts of directional drilling, sufficient fracture flow connection was successfully achieved in 1997.

The joint opening pressure of the reservoir was 10.3 MPa. Fluid flow through the reservoir was estimated to be 1300 - 2170 m^3, at near-constant flow rate of 5.7 l/s and an injection pressure of 8.3 MPa, and it produced 3-5 MW with temperature drawdown of 7 °C after 200 days of circulation.

The reservoir of Phase II was larger than of Phase I and holes had to be redrilled several times before a good connectivity was established. The second reservoir could produce 4 MW of thermal energy with injection rates of 6.3 l/s and did not show thermal drawdown after 233 days of cumulative circulation. Water loss rate of the second reservoir was approximately 7.3% of the injection rate. The joint opening pressure of the reservoir was 31 MPa, three times larger than for the Phase I. The reservoir was 200-600 meters deeper, so lithostatic pressure only accounted for 5-10 MPa. The main reason for larger required joint opening pressure was joints less favourably aligned with respect to local stress field. It is assumed that stress field remained the same at the 200 m increment. (Kelkar et al., 2016; Duchane and Brown, 2002)

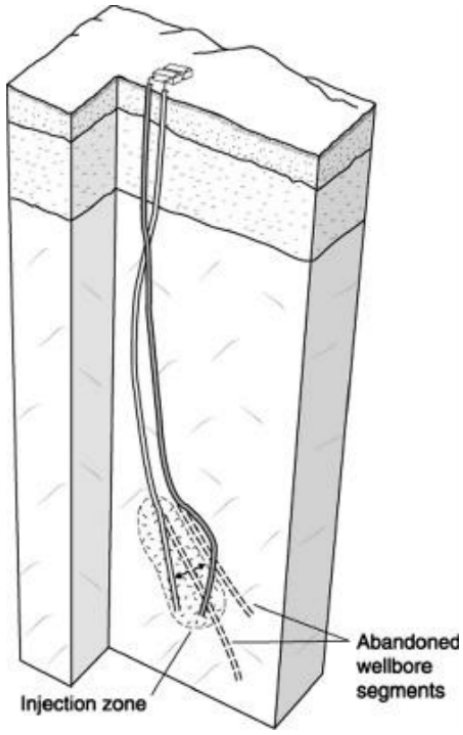

Figure 3.2: Schematic figure of Phase II drillholes. From Duchane and Brown (2002)

This pioneering work demonstrated that deep high-temperature wells can be completed in crystalline rock, and that rock can be stimulated to create hydraulically permeable fractures. The test site was shut down in 1996 but it provided with valuable knowledge about drilling and HDR energy production.

3.2.2 Soultz-sous-Forêts

The pilot EGS project in Europe was launched in 1986 in Soultz-sous-Forêts, France, as a collaboration of several European countries. The reservoir is located in Upper Rhine Graben in Paleozoic granites. The area underwent several tectonic events, and is "regarded as typical example of synorogenic intracontinental foreland rifting" (Baillieux et al., 2011). The reservoir is formed in naturally fractured and hydrothermally altered granite. Although permeability of the granite is low, it has prominent fractures of different scales and in highly fractured areas heat transfer is dominated by advection. Beneath a highly fractured layer, at depth of 3.3 km, geothermal gradient is 30°C/km (Genter et al., 2010b). The area is very favourable to EGS.

Two reservoirs were created at depths of 3.5 and 5 km. The reservoir at 3.5 km was formed first, with two wells 450 m apart, both stimulated hydraulically. Soon afterwards, a second reservoir was developed at 5 km depth by deepening one of the boreholes of the first test and drilling two

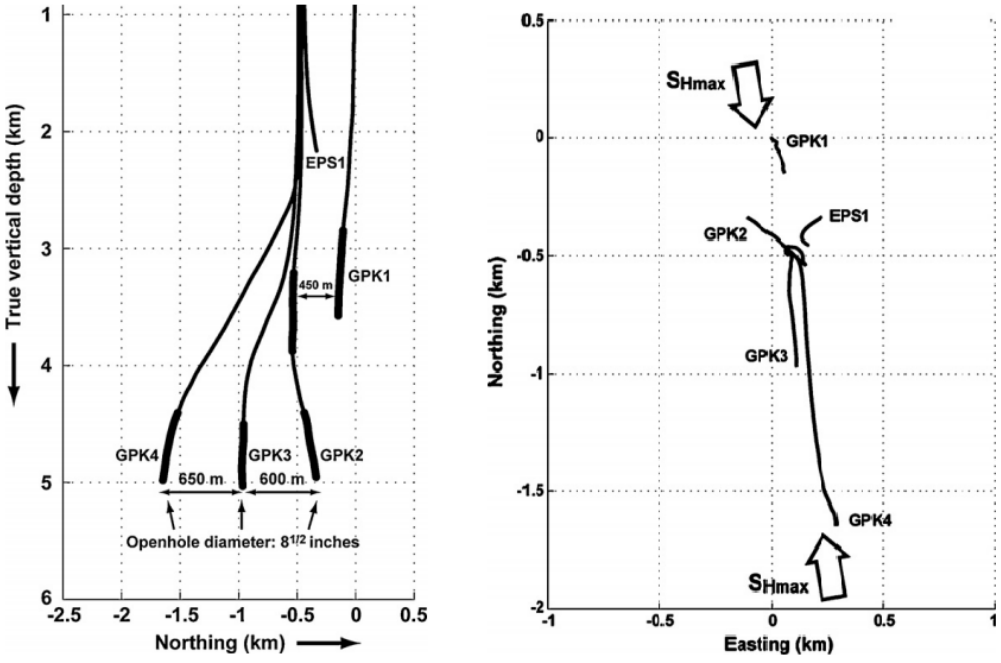

Figure 3.3: Drillhole system of Soultz reservoir at depth and projected on the surface, from Genter et al. (2010b)

more wells each 600 m apart. Besides hydraulic fracturing the fractures were stimulated by acidization injections.

The first system was tested for doublet circulation for 4 months and second system for 5 months by injecting fluid in the central well and producing from two outer wells. The first system performed well on the tests. The second system only provided good results from one well while the other production well did not link to the injection well and had to be further stimulated with acid in order to achieve high enough productivity. (Genter et al., 2010b)

The power plant was built in 2008 and organic rankine cycle (ORC) plant has production capacity of 1.5 MW electrical power (Genter et al., 2010a).

3.3 Energy production estimation

Heat extraction rate for an EGS reservoir depends on the fluid flow rate and the specific enthalpy difference between the injected and extracted fluid. The larger is the temperature difference between the ambient rock and circulated fluid, the more heat can be extracted. The risk is to cool the reservoir too rapidly. Also large temperature difference requires longer time for water to heat up to the ambient temperature. Cold water injected at high flow rate might reach the production well before heating up sufficiently.

Thermal power can be estimated using maximum mass flow rate F (in kg/s) in the reservoir with the temperature difference and specific heat capacity of fluid c_w (Lund and Freeston, 2001):

$$P = (T_i - T_a)Fc_w \tag{3.1}$$

T_i is initial reservoir temperature and T_a the theoretical base temperature to which reservoir temperature can be reduced before its efficiency decreases. This temperature is set as 80 °C as recommended in Beardsmore et al. (2010) or as 70 °C as suggested in Saadat et al. (2010).

In conditions of Southern Finland at 6 km depth the initial temperature of rock is approximately 100°C and reasonable flow rate in one fracture is 0.1 kg/s. With these parameters power production is

$$P = (100°\text{C} - 80°\text{C}) \times 1\frac{kg}{s} \times 4180\frac{J}{kgK} = 8.4kW \tag{3.2}$$

Considering that reservoir consists of a fracture system, with 100 fractures, total maximum flow rate of 10 kg/s, power production would be 0.84 MW $\approx$ 1 MW. This is the estimated energy produced from the reservoir.

3.4 Environmental impacts and sustainability

Although generally considered environmentally friendly, all renewable energy production methods have environmental impacts. The difference between *renewable* and *sustainable* is that the first one describes the nature of resource: on a short enough time scale the resource can be utilized repeatedly, the latter applies to how the resource is utilized. Fossil fuels require time scales of millions of years to form and nuclear fuel does not renew at all. Wind and sunlight as energy sources are accessible depending on the weather and climate, but practically always renewable and always sustainable.

Water sources for hydropower can decrease or dry out, if utilized excessively, and crops used for biofuels can deteriorate due to excessive land use, chemicals or climate change. Subsurface heat is renewable, but the time scale of its *renewability* depends on how sustainably it is accessed - if hot water is pumped out with too high rate, the reservoir cools down and takes decades or centuries to replenish. (Rybach, 2003)

Greenhouse gas emissions of geothermal energy are much lower than of fossil fuels (Figure 3.4) and the plant does not require any fuel (excluding energy used for pumping), and it provides locally produced energy. There are, however, emissions during the lifespan of the plant. Geothermal power

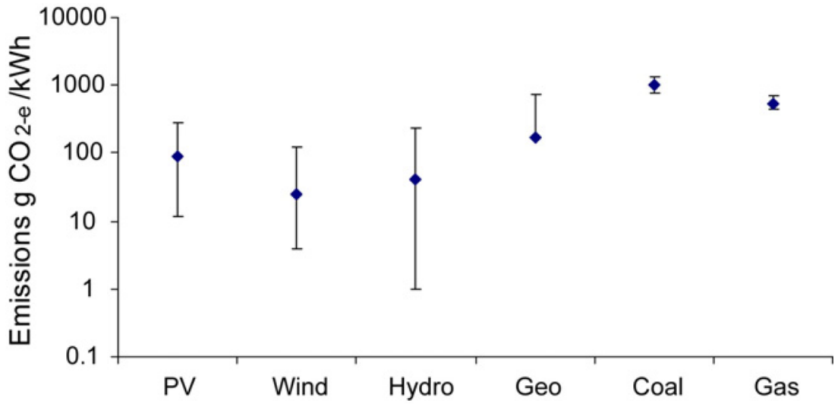

Figure 3.4: Emissions of different energy sources in carbon dioxide equivalents. From Evans et al. (2009)

plant requires electricity to operate, as well as energy required for the drilling of the wells and emissions produced during the drilling. While in operation, the plant may have environmental impacts that are discussed here:

- Air, water and noise pollution
- Induced seismicity
- Induced landslides
- Land subsidence
- Water and land use
- Cooling of the reservoir
- Disturbances in water and land habitat and vegetation

Especially pollution of surrounding air and water, including surface and groundwater has been a serious issue with early hydrothermal plants. Water circulated in the reservoir contains dissolved gases and heavy metals as well as some acid constituents. Waste water discharged to nearby watershed or artificial lake spoils surface waters and may leak to groundwater.

Acidic components corrode casings and pipelines. Pumping water up and not injecting it back induces land subsidence due to decreased pore pressure. High production rates might cause disturbances in hydrothermal manifestations, for example by drying out hot springs. All effects mentioned above are mainly issues of high temperature areas and because EGS plants are built in areas with no hydrothermal activity their working principle differs and environmental impact is smaller. (Rybach, 2003, Frick et al., 2010)

The greatest risk of environmental impacts associated with EGS occurs during well drilling and stimulation. All fluid is reinjected into the reservoir which saves water, maintains pore pressure and reduces need for waste water management. Even though an EGS plant can be considered a closed-loop system, some of the injected water is lost in the formation. Some surface water pollution can occur from surface runoff of drilling mud or leaks in the casing. Water demand of EGS is higher than of a natural hydrothermal system, and while this is not a problem in Finland, it is a serious issue in the areas where water resources are sparse. In the plants operating with steam the working fluid must be cooled to condense - this is addressed as waste heat that should be minimized. (Tester et al., 2006)

Induced seismicity occurs mainly during initial permeability enhancement but may also occur during later fluid injection. The events are mainly microearthquakes of less than magnitude of 2, but there are recorded cases of earthquakes up to magnitudes of 4-5. Hydrofracturing is, by definition, a form of induced seismicity. Water is pumped into the rock and increased local pore pressure decreases static friction and facilitates seismic slip. Tensile failure creates a "driven" fracture, and fracturing ends when pressure no longer exceeds the fracture gradient. Shear failure has also been observed in association of hydrofracturing. (Majer et al., 2007)

Other mechanisms induce seismicity besides increased pore pressure effect: decrease of temperature due to cold water injection can cause thermoelastic strain that triggers the slip. Geochemical alteration of fracture surfaces changes coefficient of friction on the surfaces. These events usually

take place at the fractures that are already near failure in a regional stress field (Majer et al., 2007). Large magnitude events require a variety of factors to come together simultaneously and therefore are not a common phenomena. Earthquakes induced by EGS are a great concern mainly because of public opinion of geothermal systems when occurring in urban areas. There might be a fear of cumulative effect or larger earthquakes and therefore open communication with local residents is necessary.

In operating EGS, pumping heat from crystalline rock causes gradual decrease in output and reservoir temperatures. Important task is to parametrize the system so that decrease is small enough during desired operation time after which the system is left to replenish. Production at lower rates prolongs lifetime of the reservoir but low production rates might not be economical. All in all, sustainability of geothermal systems is a matter of production level. (Rybach, 2003)

Chapter 4

Modelling heat and mass transfer in the fracture and surrounding rock

The models for heat flow in a fracture and around it are done analytically following the solutions of Rodemann (1979) and numerically with COMSOL Multiphysics finite element software. The aim of the models is to parametrize the system: the main parameters varied are Darcy flow velocity, size of the reservoir and permeability.

While analytical model has many simplifications, its importance is verified when correlating the models. COMSOL Multiphysics allows many modifications to the simple model and it is possible to apply different permeability distributions. Finite element model is also possible to expand to 3D, but it requires computational capacity.

The geometry of the models is visualized in Figure 4.1 as a 3D object. The calculations are performed in 2D planes in x-y and x-z directions. Calculation of temperature at the output well considers a fracture of width b (y direction) and of length L (x direction), which is the distance between injection and production well. Conduction in vertical direction from the fracture is calculated in z direction. The propagation of heat front in the fracture

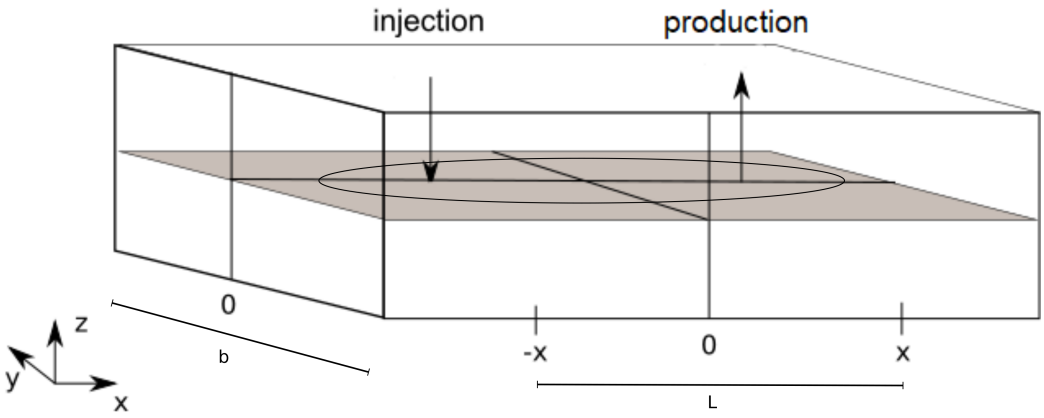

Figure 4.1: 3D model of the reservoir and surrounding rock

is on x-y plane. Here the fracture is modelled as a penny-shaped object with radius R, where R is larger than the distance between injection and production well.

Models solve the heat flow equations 2.6 and 2.8. There is assumed to be no additional heat production ($A = 0$). In the rock heat is transported only by conduction (Equation 2.7):

$$\frac{\delta T}{\delta t} = \alpha \nabla^2 T \tag{2.7}$$

In the fracture heat is transported by advection (Equation 2.8). On the fracture boundaries temperature is "recharged" from the surrounding rock. Considering fracture geometry of x-z plane of Figure 4.1, advection equation is written as given in Bodvarsson (1969) and later expanded by Gringarten and Sauty (1975) by taking porosity ϕ into account:

$$h\rho_A c_A \frac{\delta T}{\delta t} + \mathbf{q}\rho_w c_w \nabla T = \lambda \frac{\delta T}{\delta z} \tag{4.1}$$

Where

$$c_A \rho_A = (\phi - 1) c_r \rho_r + \phi c_w \rho_w \tag{4.2}$$

4.1 Analytical models

4.1.1 Equations

The analytical result for two-dimensional heat and fluid flow in a fracture as in Equation 4.1 was first presented by Bodvarsson (1969).

$$T = \Delta T_0 \; erfc\Big[(\frac{2\lambda x}{c_w h \rho_w u} + z)/2\sqrt{\alpha t}\Big] \tag{4.3}$$

Where ΔT_0 is the initial temperature difference between the injected water and host rock, λ rock thermal conductivity, c_w and ρ_w water thermal capacity and density, respectively, α rock thermal diffusivity, h is fracture aperture, u velocity of fluid and t time. It describes transient temperature change along the fracture and direction of fluid flow (x) and at certain distance perpendicular to the fracture (z). This model has great simplifications as the assumption is that the fracture is of infinite length and width, and good permeability in the fracture surrounded by impermeable rock.

The analytical model by Rodemann (1979) introduces more detailed flow taking into account not only the properties of water, but also density and specific heat capacity of rock, and rock porosity.

When solving the heat flow equation (4.1) Rodemann presents results for two geometry setups, first a 1D-result at the horizontal distance x from the injection point and vertical distance z from the fracture, and second a 2D-result of the fracture plane:

$$T = T_{ini} + \Delta T_0 \; erfc\Big[(\frac{z}{\sqrt{\alpha}} + \frac{2\sqrt{c_r \rho_r \lambda}}{c_w \rho_w} \frac{bx}{F})/\sqrt{t - \frac{c_A \rho_A}{c_w \rho_w} \frac{hbx}{F}}\Big] \tag{4.4}$$

and

$$T = T_{ini} + \Delta T_0 \; erfc\Big[(\frac{z}{2\sqrt{\alpha}} + \frac{\sqrt{c_r\rho_r\lambda}}{c_w\rho_w}\frac{S}{F})/\sqrt{t - \frac{c_A\rho_A}{c_w\rho_w}h\frac{S}{F}}\Big] \tag{4.5}$$

where S is flow geometry factor

$$S = \pi R^2 \Lambda(\xi, \theta) \tag{4.6}$$

here R is fracture radius and F flow in $\frac{l}{s}$. $\Lambda(\xi, \theta)$ is a geometry factor described below.

Together these models can build a 3D model where heat is transferred by advection in xy-direction and conduction in xz-direction.

The geometry factor Λ of Equation 4.6 was first introduced by Muskat (1937). The geometry factor describes the flow between two points in the coordinate system of equipotentials (ξ) and streamlines (θ). The coordinates are defined as functions of x and y as

$$\xi = \frac{1}{2}\log\frac{x^2 + (y-d)^2}{x^2 + (y+d)^2} \tag{4.7}$$

$$\theta = \tan^{-1}\frac{-2dx}{x^2 + y^2 - d^2} \tag{4.8}$$

where $d = L/2$ is the distance of the well from the center.

The geometry factor Λ is

$$\Lambda(\xi, \theta) = \frac{1}{\sin^2\theta}\Big[\frac{\sinh\xi}{\cos\theta\cosh\xi} - 2\cot\theta \;\tan^{-1}(\tan\frac{\theta}{2}\tanh\frac{\xi}{2}) - \frac{\sinh\xi_0}{\cos\theta\cosh\xi_0} - 2\cot\theta \;\tan^{-1}(\tan\frac{\theta}{2}\tanh\frac{\xi_0}{2})\Big] \tag{4.9}$$

where ξ_0 provides the initial position of the equipotential lines, that is the

radius of injection pipe. Λ, equipotentials and streamlines are visualized in Figure 4.2

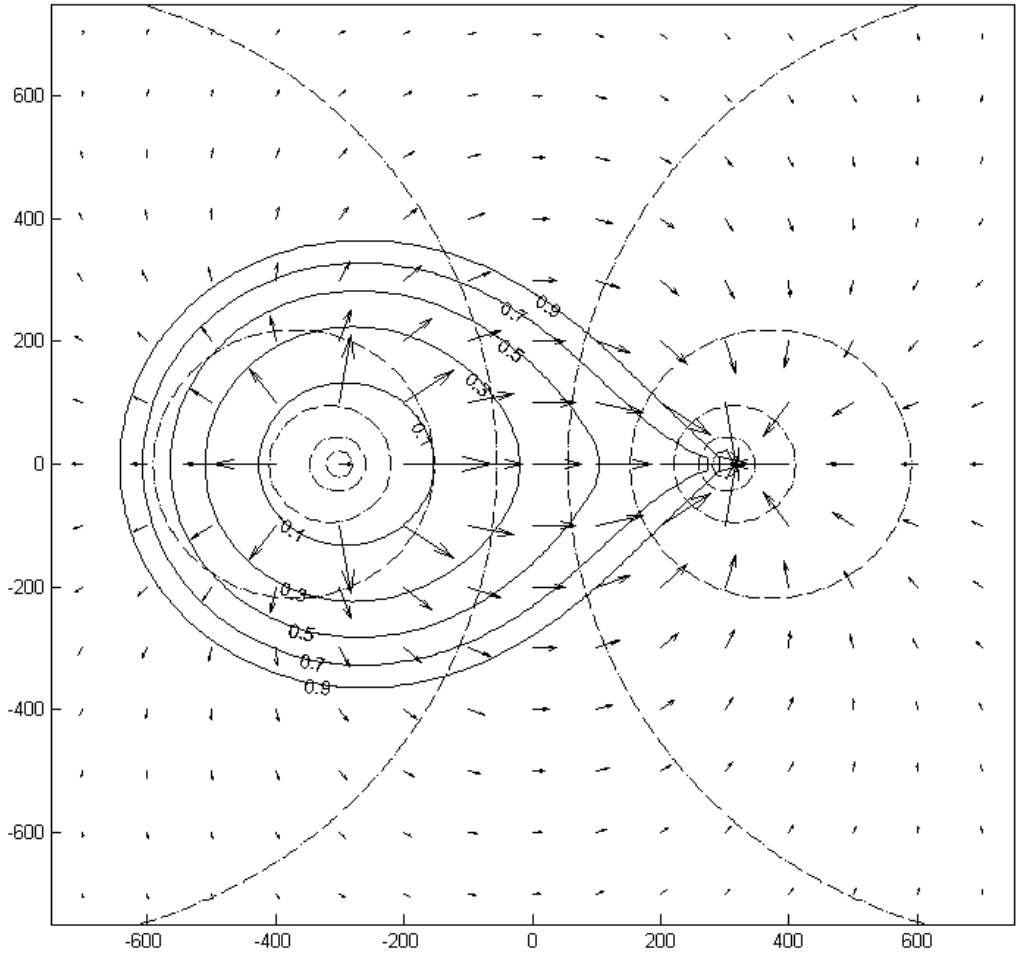

Figure 4.2: The equipotentials (dashed line), streamlines (arrows) and geometry factor Λ (solid line). Injection well is located at (x = -300; y = 0), production well is located at (x = 300; y = 0)

4.1.2 Results

Solving Equations 4.4 and 4.5 with the parameters listed in Table 4.1 provides results summarized in Figures 4.3 - 4.5. The Figure 4.3 shows fracture on the x-y plane and heat is transported through advection with water along the pattern geometry factor Λ (Figure 4.2). The Figures 4.4 - 4.5 use Equation 4.5 to plot temperatures at certain locations on x-z-plane as a function of time.

Considering constant mass flow from the injection well the flow is distributed along the reservoir as in Figure 4.2 and cold temperature of injected

Table 4.1: Total list of model parameters used in analytical and numerical models

Parameter	Value	Unit	Parameter name
T_{ini}	373.15	K	Initial temperature
T_{inj}	333.15	K	Injection temperature
t	$20 \cdot 356 \cdot 24 \cdot 3600$	s	Time
α	1.357×10^{-6}	$\frac{m^2}{s}$	Diffusivity
λ	3	$\frac{W}{mK}$	Thermal conductivity
c_w	4180	$\frac{J}{kgK}$	Specific heat capacity of water
c_r	850	$\frac{J}{kgK}$	Specific heat capacity of rock
ρ_w	1000	$\frac{kg}{m^3}$	Density of water
ρ_r	2600	$\frac{kg}{m^3}$	Density of rock
ϕ	0.01		Porosity
h	1×10^{-3}	m	Fracture aperture
r	0.01	m	Borehole radius
L	600	m	Distance of wells
R	1200	m	Reservoir radius
b	1800	m	Reservoir width
F	0.1	$\frac{kg}{s}$	Mass flow rate
v	1×10^{-3}	$\frac{m^3}{m^2 s}$	Fluid injection velocity
κ	10^{-13}	m^2	Average permeability

water is spreading into the reservoir. This spreading is referred to as cold temperature front and when water of the injection temperature reaches output well without heating on the way the situation is referred to as temperature breakthrough. Thermal breakthrough is of course not desired and the aim is to find such parameters that it does not occur. The governing parameters are the reservoir size and fluid flow velocity: the larger the distance between the wells or the lower is the mass flow the slower is the advance of thermal front.

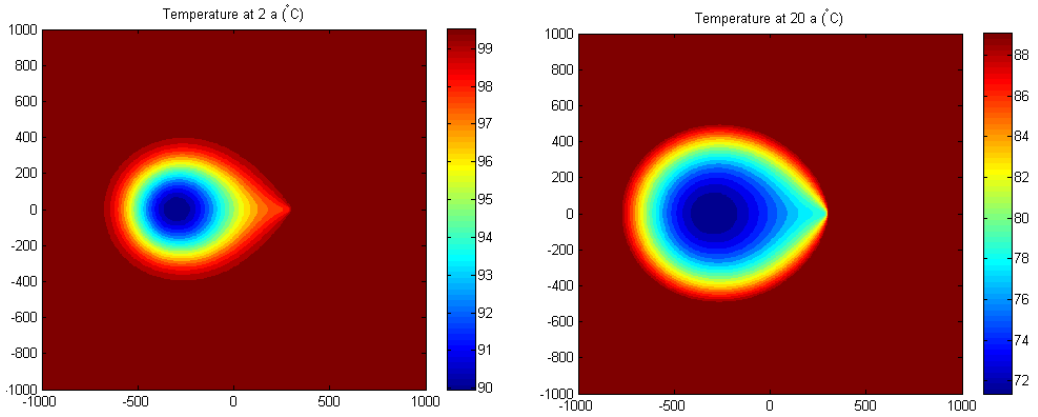

Figure 4.3: Analytical model: Flow between two wells, injection well is at (x = -300; y= 0), production well is at (x = 300; y = 0), temperature at 2 and 20 years

As seen in Figure 4.3 temperature decrease follows the predefined pattern. Due to boundary conditions, temperature of the whole reservoir decreases with time - this can be modified by editing Λ. Equation 4.4 is useful for plotting temperatures at certain distances as a function of whole operational period.

The blue line in Figure 4.5 (x=0m) shows the output temperature as a function of time. If base temperature is set to 80 °C, with used parameters the plant is productive for only 6 years. In case the plant stays productive for 20 years, the reservoir temperature will lower to 72 °C.

The curves in these figures are highly dependant on reservoir width b, which is here set as 1.5 × reservoir radius ($1.5R = 1800m$), but in reality it is most likely much smaller.

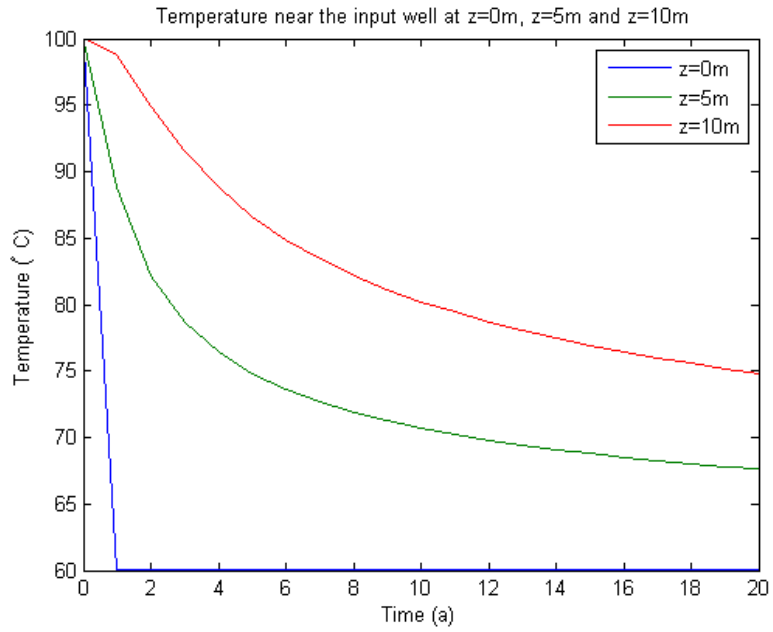

Figure 4.4: Comparison of temperatures **a)** near injection well (x = -300)

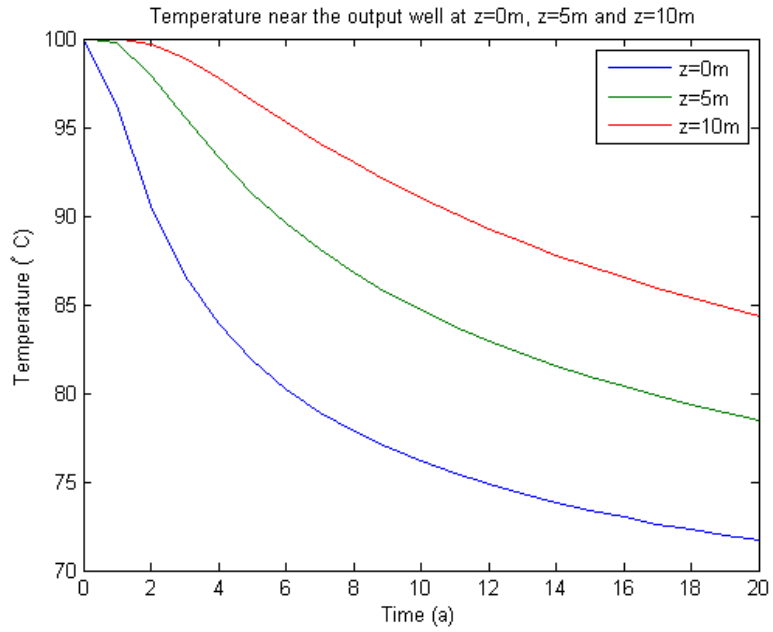

Figure 4.5: Comparison of temperatures **b)** at output well (x = 300) and at vertical distance z from it

Figure 4.4 is useful for studying at which vertical distance multiple fractures can exist without cooling the space between them too much. Depending on the base temperature that the rock is allowed to cool in order to still produce the desired heat the minimum distance of two fractures should be 10-20 m.

4.2 Numerical models

COMSOL Multiphysics is a finite element modelling software that can be efficiently used for many physical applications. The aim was to build a model that would be both light to run and representative for both large scale (over 100 meters) rock masses and small scale (1 mm) fracture flow. The modules utilised are Subsurface flow and Heat flow module. The software allows to couple models consisting of several parts along their boundary conditions. Subsurface flow module solves Darcy's law

$$\mathbf{u} = \frac{\kappa}{\mu}\frac{\delta p}{\delta x} \tag{4.10}$$

with boundary conditions of no-slip at the outer edges of the model, constant hydrostatic pressure in the reservoir and fluid injection at constant velocity at the input well and constant pressure of 1 atm at the output well.

Heat flow module solves heat and mass flow equation simplified into

$$(\phi\rho_w c_w + (1-\phi)\rho_r c_r)\frac{\delta T}{\delta t} + \rho_w c_w \mathbf{u}\cdot\nabla T = \nabla\cdot((\phi\lambda_w + (1-\phi)\lambda_r)\nabla T) \tag{4.11}$$

with boundary conditions of constant initial temperature in the reservoir and at the outer egdes of the model and cold temperature at the injection well.

2D COMSOL-models have a geometry similar to the analytic model in xy directions (Figure 4.3). First the result of analytical model is repeated and therefore the numerical model is benchmarked. The solution is compared to analytical model and both were fine-tuned to correlate.

Once the numerical model is benchmarked, it can be expanded further. The result is repeated with a model from x-z-direction, and these are possible to combine into a 3D model, but calculation of such model is computationally very heavy to perform. By applying correlated poroperm distributions (section 2.3.1) it is also possible to model fluid flow patterns with heterogeneous permeability and study how the cold temperature spreads.

4.2.1 2D models

The first model is a 2D model with two wells with geometry as in analytical solution of Rodemann (1979) (Equation 4.4). The development of temperature front is visualized in Figure 4.6. The parameters used in the model are the same as in the analytical model and they are listed in Table 1. Initial pressure used to calculate Darcy's flow is hydrostatic pressure and at the output well atmospheric pressure. Permeability is set to a constant $\kappa = 10^{-13}$.

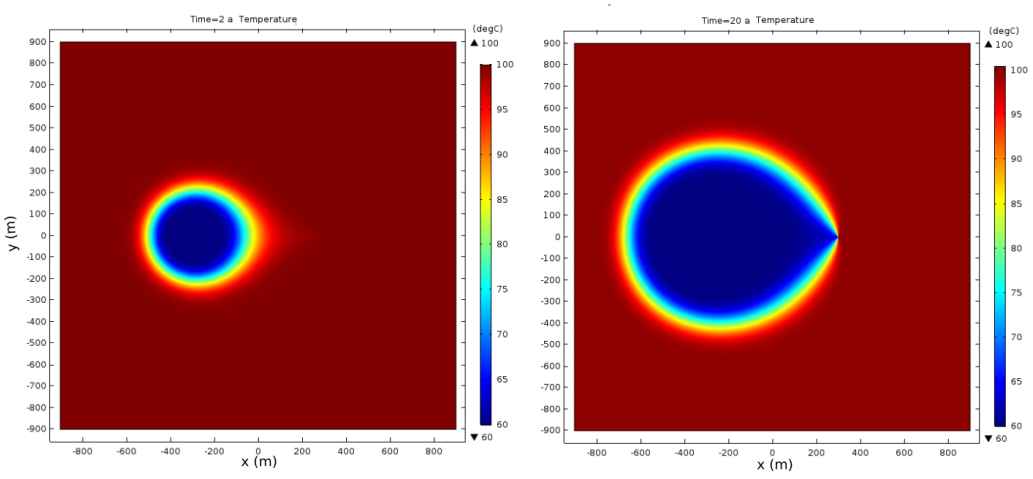

Figure 4.6: Numerical model: Flow between two wells, injection at (x = -300; y = 0), production at (x = 300, y = 0), temperature at 2 and 20 years

COMSOL Subsurface flow package has an inbuilt option for fracture flow, so this option was used to create a model with 2D flow in a single fracture in x-z-direction. This model is visualizing heat conduction in the rock matrix surrounding the fracture (similar to analytical model Equation 4.4). Fluid

flows mainly in the fracture of high hydraulic permeability ($\kappa = 10^{-13}$) and there is little flow in the surrounding rock ($\kappa = 10^{-18}$).

The model is expanded further by adding more than one fracture at vertical distance to observe how rock between the fractures cools. With fluid flow rate of 0.001 m/s cooling occurs rapidly, and at theoretical fracture distance of 15 meters temperature between the fractures near the injection wells drops from 100°C to 69°C in 4 years. However, temperature near the output wells between two fractures (x=300,y=7.5) is still relatively high 76°C.

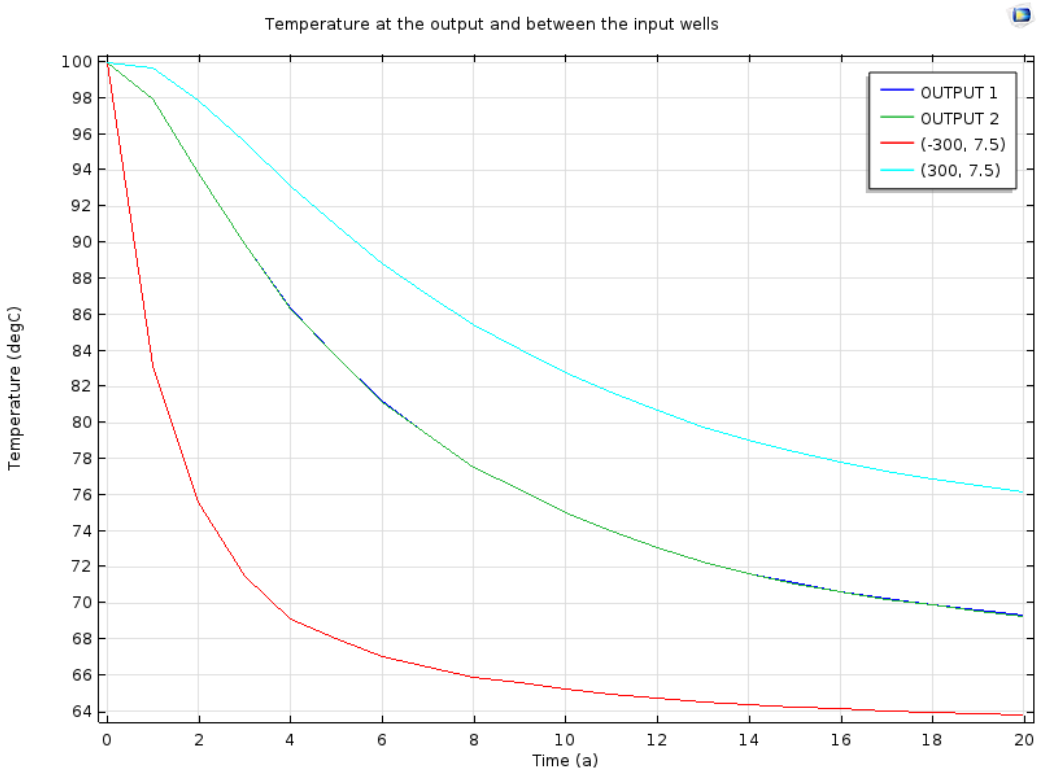

Figure 4.7: Temperatures at the output wells (x = 300; y = 7.5) and (x = 300; y = -7.5), near injection well between two fractures (x = -300; y = 0) and near a production well between two fractures (x = 300; y = 0)

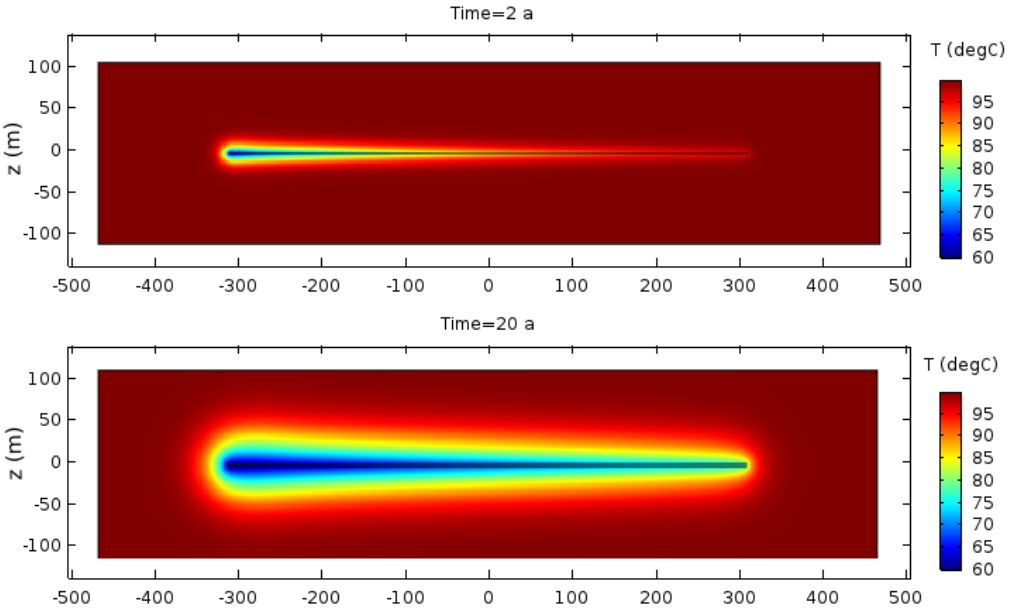

Figure 4.8: Numerical model: Heat transfer in the rock in x-z-direction with one fracture at 2 and 20 years

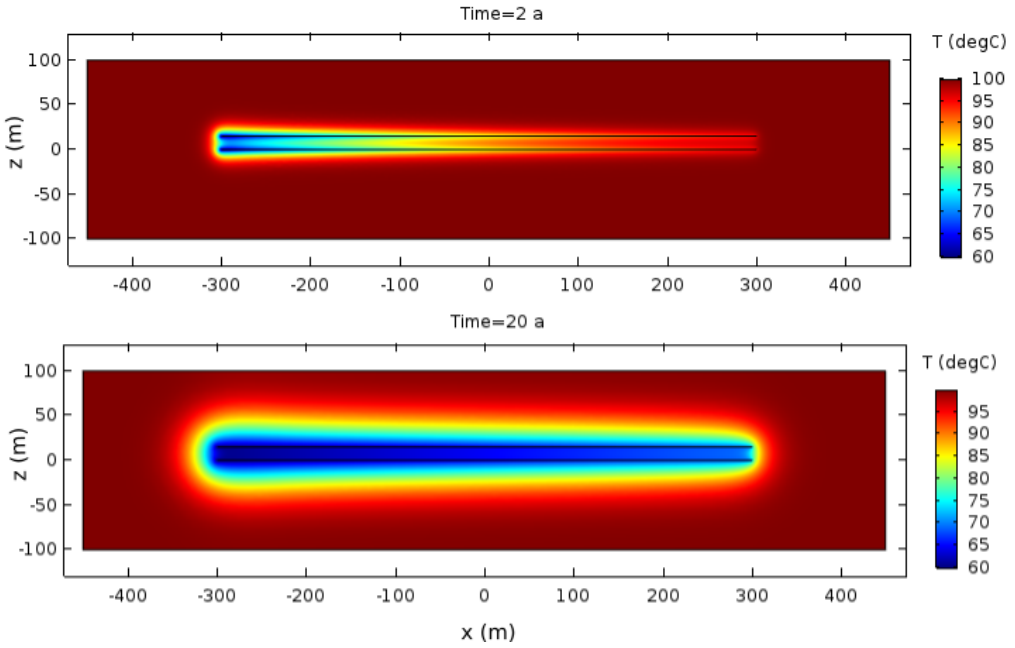

Figure 4.9: Heat transfer in the rock in x-z-direction with two fractures at vertical distance of 15 meters at 2 and 20 years

4.2.2 Heterogeneous poroperm distribution

By applying rules for spatially correlated permeability presented in section 2.3.1 it is possible to modify flow patterns. COMSOL Multiphysics is linked to Matlab by Livelink and the permeability distribution created with Matlab imported into the two-well 2D model presented above. It is also possible to initiate the permeability distribution if permeabilities at certain locations are known, for example from drillholes. Permeability distribution is initiated for $x \times y$ points, one point representing one meter. If $\kappa = e^{a\phi}$ applies for all scales, this is a valid approach, but it is still coarse estimation. Even though the distribution is spatially correlated it is still initiated as random distribution and therefore mainly suitable for studying whether output temperature is different from isotropic uncorrelated distribution presented above.

Meshing of the model plays a big role in the final distribution of permeability. Initial permeability model created with Matlab had resolution of 1 m, but meshing the numerical model had resolution of 1 m near the wells and up to 40 m at outer edges of the model. The better resolution of the mesh, the more accurate the result, but also more calculation capacity is required. Figure 4.10 shows how permeability distribution was extrapolated with coarser mesh.

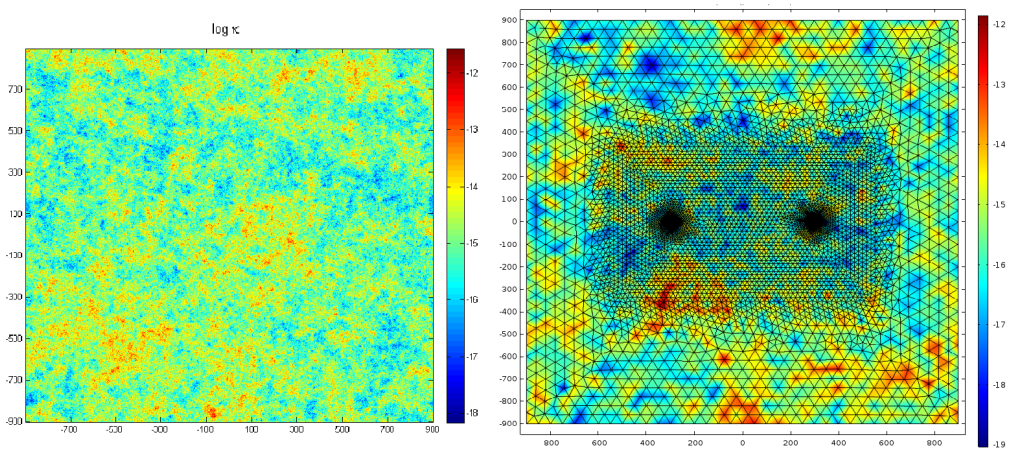

Figure 4.10: Permeability distribution created with Matlab and extrapolated permeability with model mesh created with COMSOL Multiphysics

Figures 4.11 - 4.12 present how the flow pattern and temperature change in case of certain spatially correlated distribution. Pressure builds up more in the upper part of the figure near the injection well where permeability values are low and there is higher flow rate in the lower part of the figure where permeability values are higher. Temperature of the reservoir also decreases more in the lower part of the figure.

Temperature output (Figure 4.13) is different from the model with constant permeability: the direction of breakthrough is from the bottom-left - while there is still hot water supply from the top of the figure, at the other side of the well temperature is lower. The total decrease of temperature is lower compared to Figure 4.8. This is because of lower Darcy velocity in the reservoir.

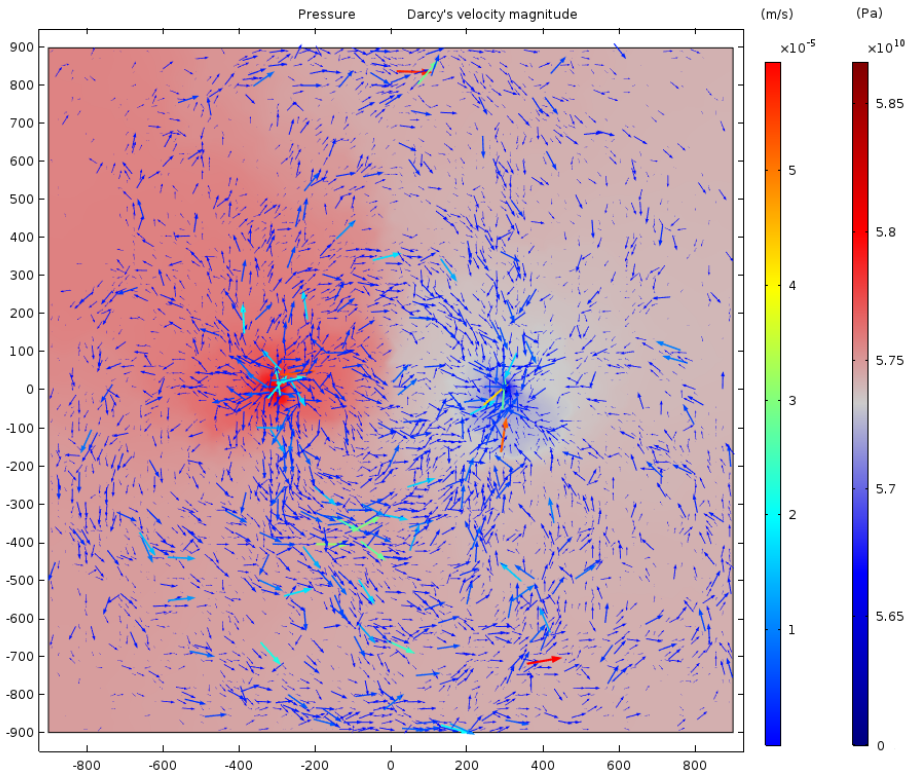

Figure 4.11: Pressure and fluid flow in the reservoir with spatially correlated permeability

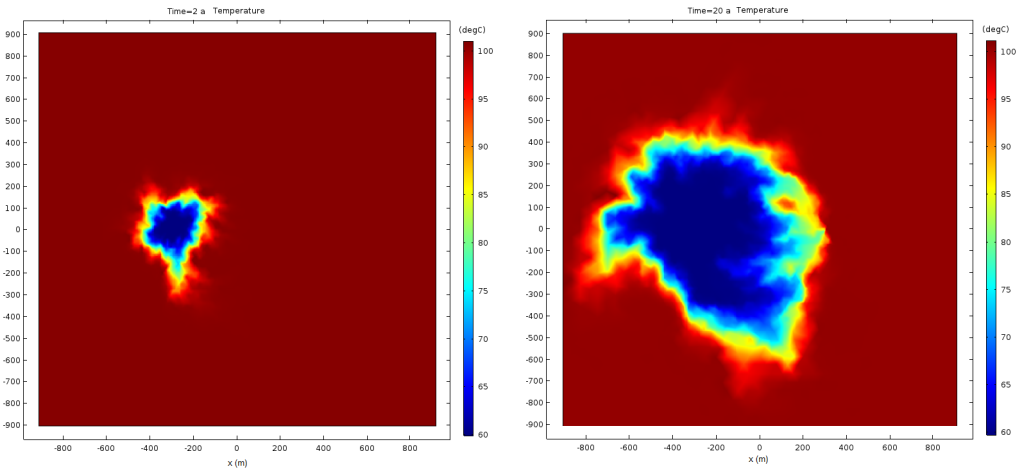

Figure 4.12: Temperature field at 2 and 20 years in the reservoir with spatially correlated permeability

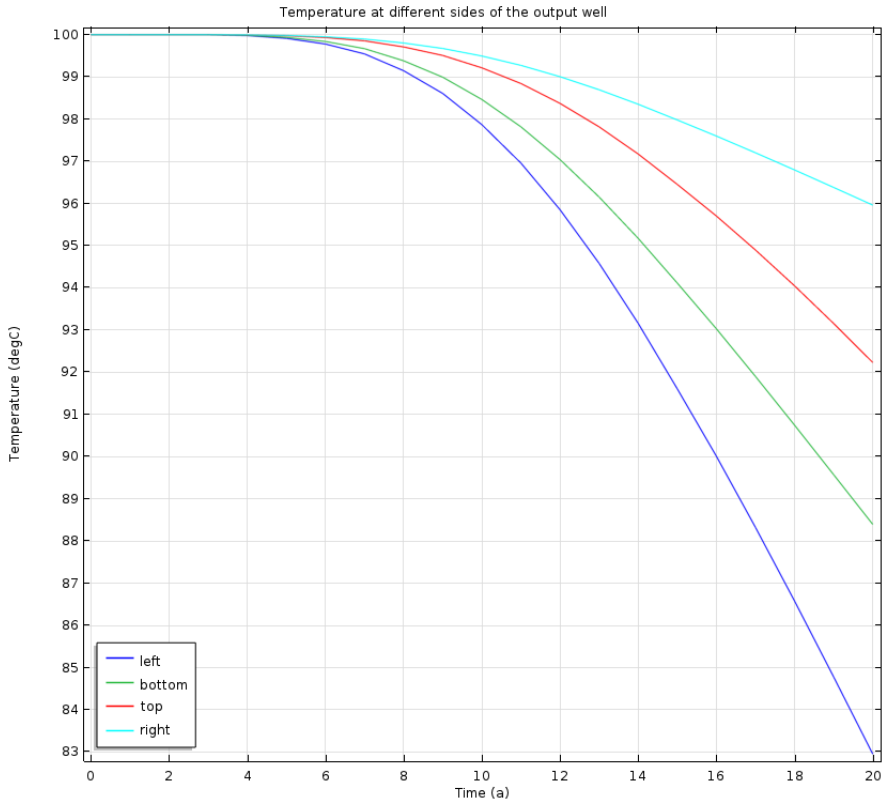

Figure 4.13: Temperature at the different sides of the output well of Figure 4.12

4.3 Correlation of analytical and numerical models

It is apparent from results of analytical and numerical models in Figures 4.3 and 4.6, that temperature distribution looks similar, and temperature breakthrough is reached at the same time with the same parameters applied. However, the "onions" are not exactly similar, this is most obvious in the figures at 2 years. In the analytical model the applied geometry factor is always of the same shape and only values inside change. Therefore cold (blue) area is small and area of gradient to the hot surrounding is large. Numerical model solves differential equation at each point of mesh grid, in result the spreading of cold front is faster and conduction has small effect - therefore change from cold to hot area is fast.

With the parameters listed in Table 4.1 temperature curves at the output well look similar (Figure 4.14). Numerical model cools slightly slower in the beginning but output after 20 years of production is slightly lower.

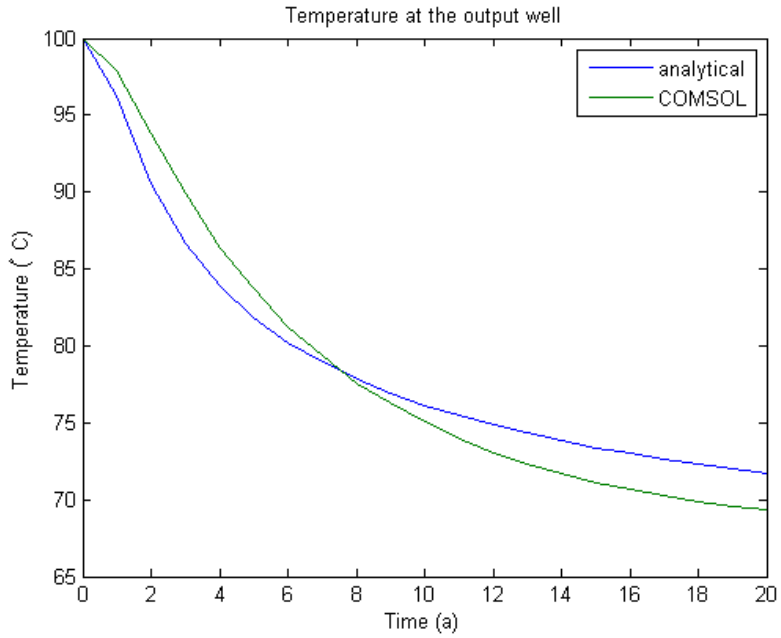

Figure 4.14: Correlation of analytical and numerical model: temperature at the output

Power production of both analytical and numerical models was studied with Equation 3.2. The result of COMSOL model is slightly more refined because c_w is a function of temperature instead of a constant value. The power production curves follow temperature curves and give very similar results.

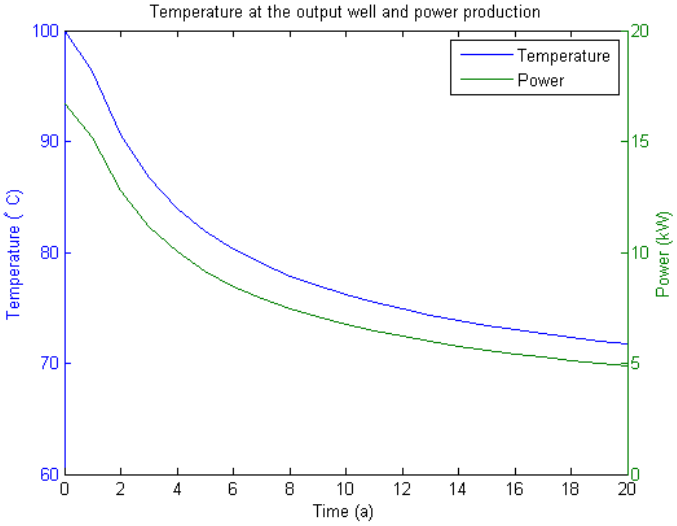

Figure 4.15: Analytical model: output temperature and power production

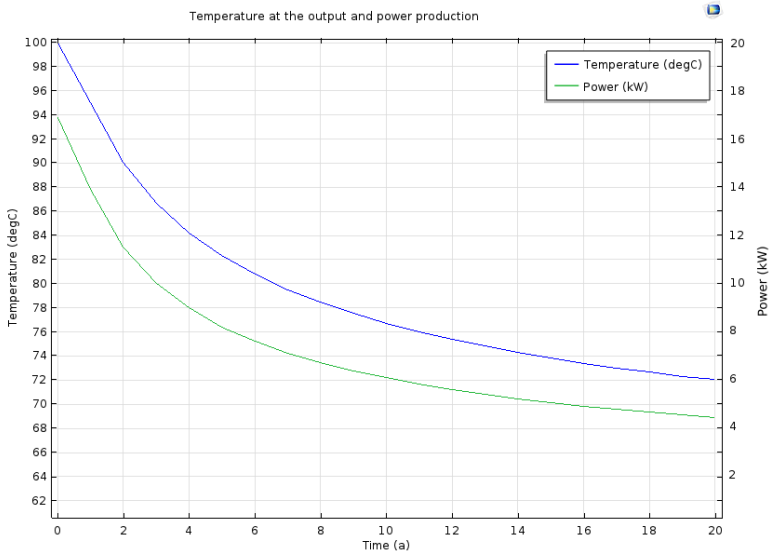

Figure 4.16: Numerical model: output temperature and power production

COMSOL faced convergence issues when running a model with parameters that caused too large pressure gradients. At low permeability values ($\kappa < 10^{-18}$) fluid flow did not take place at all, and at very high permeability ($\kappa > 10^{-10}$) calculation did not converge. Since Rodemann solutions do not take permeability into consideration, this was not an issue with the analytical models.

Chapter 5

Discussion and conclusions

The numerical models presented here can be further developed into different 3D setups with multiple fractures so that cumulative flow is sufficient, but this requires more computational power. The model does not take into account changes in fluid temperature while it is being pumped up to the power plant and down to the reservoir.

The results of the models show that with the chosen parameters achieving sustainable production for more than 10 years is only possible with a large reservoir and low flow velocity. Such parameters are unrealistic - reservoir as large as of 1 km in diameter is hard to create even at small depths with more permeable rock, not to mention complications brought by 7 kilometres of rock on top. At low fluid flow rate ($u < 0.001 m/s$) production is not feasible and very likely injected fluid will never reach production well but will be lost to the outside of the reservoir. Also, an important task of injected fluid is to maintain sufficient permeability, so at low fluid rates the created permeability will probably not be sustained.

Calculations of power production show that with the reservoir parameters presented in Table 4.1 the power possibly produced from the system is around 1 MW (Equation 3.2). This is similar to 1.5 MW of Soultz, but falls short from estimated 40 MW that the energy company ST1 has been promoting (*ST1 Deep Heat project website*). In order to achieve higher power production

the temperature difference should be larger, but in the given regime it would require drilling deeper, which is complicated and not economically feasible. If fluid is circulated at higher fluid flow rate or with colder water input, the reservoir cools down very fast.

As a conclusion, the models created for this thesis show that creating several fractures with spacing of 15 m and circulating fluid with the parameters used in the models can only produce enough thermal energy for short time. With high fluid flow the reservoir cools too rapidly and output fluid temperature is not sufficiently high.

When spatially correlated permeability is applied, total permeability average should remain similar to the constant permeability of homogeneous models. If this condition fails and average permeability is lower than in homogeneous permeability models, Darcy flow velocity in the reservoir is slower and output temperature decreases less than with homogeneous permeability. Theoretically, power production is higher in this case.

5.1 Options

There are other possible well-reservoir geometries that could work for a specific site. One option is to shift the system to lower depth and use heat pumps to increase the temperature of production fluid. Low depth wells have an economical benefit: with the same price as two 7 km deep holes, several holes of for example 3-4 km can be drilled. Initial permeability is higher (Figure 2.2) at 4 km depth and pressure is lower, which makes hydraulic stimulation easier.

With more boreholes there is higher possibility to obtain good connectivity. There can be two or more production wells around the injection well as in Soultz (Chapter 3.2.2). This way stimulation of fractures can be done from multiple wells and the reservoir can be utilized more efficiently.

Boreholes are often directed to be perpendicular to the minimum principle stress. In case the least principal stress is vertical, the reservoir can

be formed between two or more horizontal wells that are drilled from the opposite directions. Such formation is called a "radiator" concept.

Due to the distinctive requirements of each site the geometry should always be accessed individually according to the local geology and stress regime.

5.2 Conclusions

This thesis provides a brief outlook of ongoing work with Enhanced Geothermal Systems. Geothermal energy is a growing industry and with EGS technology it is possible to utilize geothermal energy in low heat flow areas. Space heating and cooling create a large demand for energy and geothermal heat enhanced with heat pumps reduces the need for fossil fuels.

The ongoing EGS project in Southern Finland provides a great opportunity to learn and explore EGS technologies in a complex environment: hard crystalline rock, high pressure and low permeability. In this work I describe physics behind an EGS plant, as well as basic concept of EGS, give examples of some existing plants and make calculations of how much power a plant in Finland can produce. In order to plan and build a successful plant, suitable parameters for the system are determined by modelling.

Physical properties governing the EGS models are conductive and convective heat transfer and rock hydraulic properties that allow fluid flow. Equation for conservation of thermal energy and continuity equation presented in Chapter 2 are solved with suitable boundary conditions in Chapter 4. Hydraulic permeability is discussed in detail, because it is the key parameter in EGS: rock is stimulated in order to enhance permeability in order to make fluid flow possible through interconnected fractures.

Permeability decreases with depth due to increasing pressure. Permeability can be quantified by empirical laws determined by Leary et al. The laws state that 1. well-log spectra S correlate inversely with with spatial frequency k over scale lengths of five orders of magnitude $(1/km - 1/cm)$,

2. fluctuations in well-core porosity ϕ scale to the fluctuations in logarithm of permeability κ and 3. permeability is a function of exponent of porosity multiplied by empirical integration constant a.

By utilizing these laws EGS reservoir permeability can be modelled as spatially correlated medium with lognormal distribution of permeability: there are few channels that a lot of fluid flows through and many channels that barely permit any fluid through.

Modelling of heat and mass transfer aims to parametrize an EGS plant in the conditions of Southern Finland. Low geothermal gradient requires drilling deep in order to achieve temperature feasible for production. Lithostatic pressure increases with depth and decreases permeability. The parameters governing heat transfer with fluid flowing in the geothermal reservoir are size of the reservoir and fluid velocity, which depends on matrix permeability. The larger the reservoir the more hot contact area the fluid encounters and the better it heats up, the slower the flow, the longer time fluid stays in the reservoir and therefore heats up more. High flow rates cool the reservoir rapidly. However, a large reservoir is difficult to achieve, maintaining enhanced permeability requires relatively high fluid flow rates and the higher the flow rate, the more power the plant produces, so slow flow is not economically feasible.

The modelling in done analytically and numerically. Analytical models use solutions of Rodemann (1979) and create flow pattern with uniform permeability. Numerical models are made with COMSOL Multiphysics and the models solve differential equations introduced in Chapter 2. First numerical model is done to reproduce results of analytical model. Further models use spatially correlated permeability to modify fluid flow pattern and see how temperature in the reservoir changes with changes in fluid flow.

The results show that creating large reservoir that could operate for 20 years with desired power production is unrealistic. Mass flow rate required to produce over 1 MW power is 10 kg/s with 100 fractures with spacing of 15 meters. At higher fluid flow rate or less fractures closer to each other the

reservoir cools and output fluid temperature is not sufficient. With spatially correlated permeability total fluid flow of the reservoir is slower than with homogeneous permeability and there is a risk of poor connectivity. In this case the temperature decreases less but due to low flow rate this kind of reservoir produces less energy.

The benefit of the created models is that they are adjustable to different boundary conditions (initial temperature and pressure, depth, injection fluid velocity), so they can be used in many possible regimes. Spatially correlated permeability can be initiated if permeability at certain locations is know from *in situ* measurements.

As an option to the plant parameters obtained in these models, different geometries are discussed. Feasible production could be obtained by creating a smaller reservoir at lower depths and increasing temperature with heat pumps. In case of creating reservoir at initially planned depth, the size of created reservoir will likely be tens and not hundred meters of radius, and temperature will be, again, increased to desire output with heat pumps

Bibliography

Anderson (1951): *The dynamics of faulting and dyke formation with applications to Britain*. Edinburgh: Oliver and Boyd.

Armansson, H. and H. Kristmannsdóttir (1992): "Geothermal environmental impact". *Geothermics* 21, pp. 869–880.

Arriaga, M.-C. S. and F. Samaniego (2012): "Deep geothermal reservoirs with water at supercritical conditions". *Proceedings, Thirty-Seventh Workshop on Geothermal Reservoir Engineering*, pp. –.

Baillieux, P., E. Schill, and C. Dezayes (2011): "3D Structural regional model of the EGS Soultz site (Northern Upper Rhine Graben, France): insights and perspectives". *Proceedings, Thirty-Sixth Workshop on Geothermal Reservoir Engineering*.

Bear, J. (1973): *Dynamics of Fluids in Porous Media*. American Elsevier. ISBN: ISBN 0-444-00114-X.

Beardsmore, G. R. et al. (2010): "A Protocol for Estimating and Mapping Global EGS Potential". *GRC Transactions* 34.

Bodvarsson, G. (1969): "On the Temperature of Water Flowing through Fractures". *Journal of geophysical Research* 74.3, pp. 1987–1992.

Brown, D. W. et al. (2012): *Mining the Earth's heat: hot dry rock geothermal energy*. Ed. by V. T. Hriscu. Springer-Verlag Berlin Heidelberg. ISBN: ISBN 978-3-540-67316-3.

Bruhn, D. et al. (2010): "Chapter 2: Exploration methods". *Geothermal Energy Systems*. Ed. by E. Huenges.

Carslaw, H. and J. Jaeger (1959): *Conduction of Heat in Solids*. 2nd ed. Oxford science publications. ISBN: ISBN 0-19-853368-3.

Crampin, S. (1994): "The fracture criticality of crustal rocks". *Geophysical journal international* 118, pp. 428–438.

Duchane, D. and D. Brown (2002): "Hot dry rock (HDR) geothermal energy research and development at Fenton Hill, New Mexico". *GHC Bulletin*.

Evans, A., V. Strezov, and T. J. Evans (2009): "Assessment of sustainability indicators for renewable energy technologies". *Renewable and Sustainable Energy Reviews* 13, pp. 1084–1088.

Fowler, M. (2005): *The Solid Earth: an introduction to global geophysics*. 8th ed. Cambridge University Press. ISBN: ISBN 0-521-89307-0.

Frick, S. et al. (2010): "Chapter 7: Economic Performance and Environmental Assessment". *Geothermal Energy Systems*. Ed. by E. Huenges.

Fridleifsson, I. (1998): "Direct use of geothermal energy around the world". *Geo-Heat Center Bulletin* 19.2.

Genter, A. et al. (2010a): "Contribution of the exploration of deep crystalline fractured reservoir of Soultz to the knowledge of enhanced geothermal systems (EGS)". *Comptes Rendus Geoscience* 342, 502 — 516.

Genter, A. et al. (2010b): "Current status of the EGS Soultz geothermal project (France)". *Proceedings World Geothermal Congress*.

Goldstein, B. et al. (2011): *Geothermal Energy, IPCC Special Report on Renewable Energy Sources and Climate Change Mitigation*. Ed. by O. Edenhofer et al. Cambridge University Press. ISBN: ISBN 978-1-107-02340-6.

Gringarten, A. C. and J. P. Sauty (1975): "A theoretical study of heat extraction from aquifers with uniform regional flow". *Journal of geophysical research* 80, pp. 4956 –4962.

Hubbert, M. K. and W. W. Rubey (1959): "Role of fluid pressure in mechanics of overthrust faulting: parts I and II". *Bulletin of geological society of America* 70, pp. 115–166.

IEA (2017): *Renewables Information 2017*. Tech. rep. Free excerpt. Internation Energy Agency Publications.

Ingebritsen, S. and C. Manning (1999): "Geological implications of a permeability-depth curve for the continental crust". *Geology* 27, pp. 1107–1110.

Ingebritsen, S., W. Sanford, and C. Neuzil (2008): *Groundwater in Geologic Processes*. 3rd ed. Cambridge University Press. ISBN: ISBN 978-0-521-60321-8.

Kelkar, S., G. WoldeGabriel, and K. Rehfeldt (2016): "Lessons learned from the pioneering hot dry rock project at Fenton Hill, USA". *Geothermics* 63, pp. 5–14.

Leary, P. and F. Al-Kindy (2002): "Power-law scaling of spatially correlated porosity and log(permeability) sequences from north-central North Sea Brae oilfield well core". *Geophys. J. Int.* 148, pp. 426–442.

Leary, P. et al. (2014): "Lognormality, $\delta\kappa \sim \kappa\delta\phi$, EGS, and All That". *Proceedings, Thirty-Ninth Workshop on Geothermal Reservoir Engineering*.

Leary, P. et al. (2015): "Flow Lognormality and Spatial Correlation in Crustal Reservoirs – I: Physical Character & Consequences for Geothermal Energy". *Proceedings World Geothermal Congress 2015*.

Leary, P. et al. (2017): "Calibrating the EGS flow stimulation process for basement rock". *unpublished*.

Ledru, P. and L. G. Frottier (2010): "Chapter 1: Reservoir definition". *Geothermal Energy Systems*. Ed. by E. Huenges.

Ljunggren, C. et al. (2003): "An Overview of Rock Stress Measurement Methods". *International Journal of Rock Mechanics and Mining Sciences* 40, pp. 975–989.

Líndal, B. (1973): "Industrial and other applications of geothermal energy". *Geothermal energy, Review of research and development*. Ed. by C. Armstead.

Lund, J. (2007): "Characteristics, development and utilization of geothermal resources". *Geo-Heat center quaterly bulletin* 28, pp. 1–9.

Lund, J. and D. Freeston (2001): "World-wide uses of geothermal energy 2000". *Geothermics* 30, pp. 29–68.

Majer, E. et al. (2007): "Induced seismicity associated with Enhanced Geothermal Systems". *Geothermics* 36, pp. 185–222.

Malin, P. et al. (2015): "Flow Lognormality and Spatial Correlation in Crustal Reservoirs – II: Where-to-Drill Guidance via Acoustic/Seismic Imaging". *Proceedings World Geothermal Congress 2015*.

Manning, C. and S. Ingebritsen (1999): "Permeability of the continental crust: Implications of geothermal data and metamorphic systems". *Geophysics* 37, pp. 127–150.

Muskat, M. (1937): "The flow of homogenous fluids through porous media".

Pogacnik, J. et al. (2015): "Flow Lognormality and Spatial Correlation in Crustal Reservoirs – III: Natural Permeability Enhancement via Biot Fluid-Rock Coupling At All Scales". *Proceedings World Geothermal Congress 2015*.

Rodemann, H. (1979): "Bericht über Modellrechnungen zum Wärmeaustausch in einem Frac". *Niedersächsisches Landesamt für Bodenforschung Hannover*.

Rybach, L. (2003): "Geothermal energy: sustainability and the environment". *Geothermics* 32, pp. 463–470.

Saadat, A. et al. (2010): "Chapter 6: Energetic Use of EGS Reservoirs". *Geothermal Energy Systems*. Ed. by E. Huenges.

Schulte, T. et al. (2010): "Chapter 4: Enhancing Geothermal Reservoirs". *Geothermal Energy Systems*. Ed. by E. Huenges.

Sperber, A., I. Moeck, and W. Brandt (2010): "Chapter 3: Drilling into Geothermal Reservoirs". *Geothermal Energy Systems*. Ed. by E. Huenges.

ST1 Deep Heat project website. accessed 4.10.2017. URL: `http://www.st1.fi/uusiutuva-energia`.

Stüwe, K. (2007): *Geodynamics of the lithosphere, Quantitative description of geological problems*. Springer-Verlag.

Tenzer, H. (2001): "Development of Hot dry rock technology". *Geo-Heat Center Quarterly Bulletin* 28.

Tester, J. et al. (2006): *The future of Geothermal Energy, Impacts of Enhanced Geothermal Systems (EGS) on the United States in the 21st century*. Ed. by R. Baria et al. Massachusetts Institute of Technology. ISBN: ISBN 0-615-13438-6.

Turcotte, D. and G. Schubert (2002): *Geodynamics*. 2nd ed. Cambridge University Press. ISBN: ISBN 9780521661867.

Whitaker, S. (1986): "Flow in Porous Media I: A Theoretical Derivation of Darcy's Law". *Transport in Porous Media* 1, pp. 3–25.

Zoback, M. et al. (2003): "Determination of stress orientation and magnitude in deep wells". *International Journal of Rock Mechanics and Mining Science* 40, pp. 1049–1076.